JKU
JOHANNES KEPLER
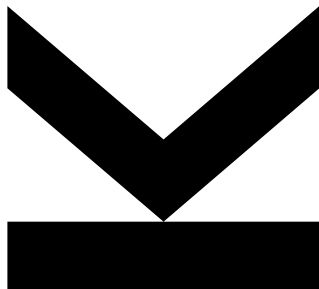## UNIVERSITY LINZ

Author
Katharina Matura

Submission
Institute of Physical Chemistry and Linz Institute of Organic Solar Cells

Thesis Supervisor
a. Univ. Prof. Dr. Markus Scharber

Thesis Co-Supervisor
DI Felix Mayr

November 2021

Embedding of highly-fluorescent perovskite nanoparticles into transparent polymeric matrices

Bachelor's Thesis

to obtain the academic degree of

Bachelor of Science (BSc)

in the Bachelor's Program

Chemistry and Chemical Technology

SWORN DECLARATION

I hereby declare that the thesis submitted is my own unaided work, that I have not used other than the sources indicated, and that all direct and indirect sources are acknowledged as references.

St.Valentin, 07.11.21

Place, Date

Signature

Acknowledgement

First of all, I would like to express my sincere gratitude to o. Univ.-Prof. Mag. Dr. DDr. h.c. Niyazi Serdar Sariciftci for encouraging and inspiring me to pursue science. I am especially thankful for giving me the opportunity to work at the Linzer Institute for Organic Solar Cells (LIOS) as well as to be so openly accepted as LIOS team member.

I would like to offer my special thanks to my co-supervisor DI Felix Mayr for his guidance, great support and for giving me inputs for a basis and deeper knowledge in the entire field. Thank you, for the most pleasant conversations making measurement hours elapse like minutes, for helping me with any upcoming problem and for being such a motivated as well as inspiring scientist.

Furthermore, I would like to express my deep gratitude towards a. Univ. Prof. Dr. Markus Scharber for his guidance during my work, his aid during measurements and for extremely interesting scientific conversations and discussions.

I would also like to thank BSc Elisabeth Leeb, who has fabricated PNP batches for my work whenever needed.

I am very grateful for every member of the LIOS team since they have made me feel so welcome in this institute. Thank you for the fun time we had in the big and the small student's office and for being not only helping colleagues but lovely friends.

Lastly, my family and friends deserve a special thank you: my family for unconditionally supporting me during my whole life and providing me perfect studying conditions and my friends for being so supportive, constructive and encouraging!

Abstract

Over the years, highly-fluorescent lead-halide perovskite nanoparticles (PNPs) have become of great interest in the field of electronics and photonics due to the wide range of optoelectronic applications. The embedding of these nanostructured particles into a protective polymeric matrix allows an improvement of their optical stability as well as a fine distribution of the particles which enables the investigation of concentration effects in solid-state thin films. The aim of this thesis was to find a compatible transparent polymer that allows to finely distribute and homogenously encapsulate highly-photoluminescent formamidinium lead bromide ($FAPbBr_3$) and methylammonium lead bromide ($MAPbBr_3$) PNPs. Furthermore, the photoluminescent properties of the prepared PNP-polymer films should be examined with the main focus lying on the investigation of effects from the PNP concentration and agglomeration. The results of this study exhibit that PNPs dispersed in toluene show a good compatibility with polystyrene or polymethyl methacrylate. However, for as-synthesized nanoparticles an unfavourable strong PNP cluster formation in the PNP-polymer films was observed. Thus, different treatment methods for the reduction of the PNP agglomeration were investigated. By a short-time redispersion in tetrahydrofuran, large PNP agglomerates could be significantly reduced in size without altering the initial high-quality photoluminescence properties of the untreated PNPs. Using this treatment method, PNP-polymer films were prepared which showed a finer and more homogenous PNP distribution as well as a good optical stability. Moreover, for these PNP-polymer films a slight increase in photoluminescence lifetime was observed when decreasing the PNP concentration. These findings demonstrate the great potential of PNP-polymer films being a basis for further studies of concentration dependent effects as well as for the examination of PNPs at a single-particle level.

Kurzfassung

Stark fluoreszierende Bleihalogenid-Perowskit-Nanopartikel (PNPs) haben über die Jahre immer mehr Interesse in den Forschungsfeldern der Elektronik und Photonik erregt, da die Nanopartikel in einer Vielzahl an optoelektronischen Anwendungen eingesetzt werden können. Durch die Einbettung dieser Nanopartikel in eine schützende Polymermatrix, kann einerseits die optische Stabilität der PNPs erhöht werden und andererseits können Konzentrationseffekte in festen Dünnschichtfilmen untersuchen werden. Das Ziel dieser Arbeit war es, ein kompatibles transparentes Polymer zu finden, in dem man Formamidiniumbleibromid (FAPbBr$_3$) und Methylammoniumbleibromid (MAPbBr$_3$) PNPs fein und homogen verteilt einbetten kann. Weiters wurden die photolumineszierenden Eigenschaften der hergestellten PNP-Polymerfilme untersucht, wobei der Schwerpunkt der Untersuchung auf den Effekten der PNP-Konzentration und Agglomeration. Die Studie zeigte eine gute Kompatibilität von PNPs dispergiert in Toluol mit den Polymeren Polystyrol und Polymethylmethacrylat, jedoch war beim Einsatz von PNPs ohne Vorbehandlung ein starkes Auftreten von großen PNP-Agglomeraten im Film zu beobachten. Daher wurden verschiedene Vorbehandlungsmethoden für die Verringerung der PNP-Agglomeration untersucht. Durch die kurzzeitige Redispergierung in Tetrahydrofuran konnten große PNP-Agglomerate deutlich verkleinert werden, ohne dabei die ursprünglichen hochwertigen Photolumineszenz-Eigenschaften der PNPs zu verändern. Mit dieser Vorbehandlungsmethode konnten PNP-Polymerfilme hergestellt werden, die eine feinere und homogenere PNP-Verteilung, sowie zusätzlich eine gute optische Stabilität aufwiesen. Darüber hinaus wurde bei diesen PNP-Polymerfilmen eine leichte Erhöhung der Photolumineszenz-Lebensdauer bei einer Verringerung der PNP Konzentration beobachtet. Diese Ergebnisse demonstrieren das große Potential von diesen PNP-Polymerfilmen, als Grundlage für weitere Studien zu konzentrationsabhängigen Effekten sowie für die Untersuchung von PNPs auf Einzelpartikelebene zu dienen.

Content

List of Abbreviations

ACN	Acetonitrile
CCD	Charge-coupled device
$CHCl_3$	Chloroform
DCM	Dichloromethane
DMSO	Dimethyl sulfoxide
Et_2O	Diethyl ether
EtOH	Ethanol
$FAPbBr_3$	Formamidinium lead bromide
FRET	Förster resonance energy transfer
H_2O	Water
IFE	Inner filter effect
LT	Lifetime
$MAPbBr_3$	Methylammonium lead bromide
MeOH	Methanol
PEG	Polyethylene glycol
PL	Photoluminescence
PLQY	Photoluminescence quantum yield
PMMA	Poly(methylmethacrylate)
PMT	Photo-multiplier tube
PNP	Perovskite nanoparticle
PPMS	Physical property measurement system
i-PrOH	2-Propanol
PS	Polystyrene
PVDF	Poly(vinylidene fluoride)
PVOH	Poly(vinyl alcohol)
PVP	Poly(vinylpyrrolidone)
QD	Quantum dot
TCSPC	Time-correlated single photon counting
THF	Tetrahydrofuran

List of Figures

List of Tables

1. <u>Introduction</u>

1.1. Time-correlated single photon counting

Time-correlated single photon counting is a useful method to measure fast relaxation processes of electronically excited materials. When a molecule is electronically excited to a higher molecular quantum state, it is energetically unstable, and the molecule will spontaneously lose the gained energy to reach the ground state again. One of the possibilities to release the surplus of energy is by radiative emission, whereby the excited state has equal spin multiplicity as the lower state reached upon relaxation. This radiative emission is called fluorescence. Moreover, the emission of fluorescence is an extremely fast happening process, which typically has a lifetime of picoseconds up to microseconds[1]. With conventional measurement techniques it is not possible to properly resolve this fluorescence decay, hence time-correlated single photon counting is the method of choice. In contrast to typical photoluminescence spectroscopy, the sample is irradiated with a periodically pulsed laser and multiple measurement cycles are conducted. The measurement is carried out via a start-stop-time measurement principle, whereby the recorded time equals the time difference between excitation laser pulse and detected fluorescence photon (see **Figure 1**)[2].

The time measurement starts, when the laser emits photons and it is finished, when a photon arrives at the detector, as can be seen in **Figure 2**. Thereby, one detected photon corresponds to one count. Consequently, a histogram of detected photons versus time difference can be constructed from the multiple measurement cycles[2].
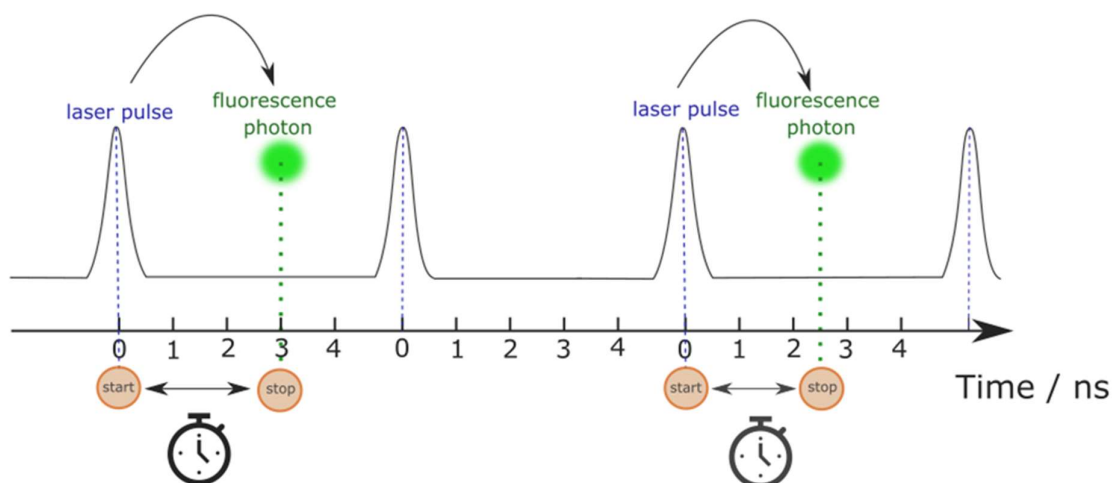
Figure 1. Scheme of the TCSPC principle adapted from [2].
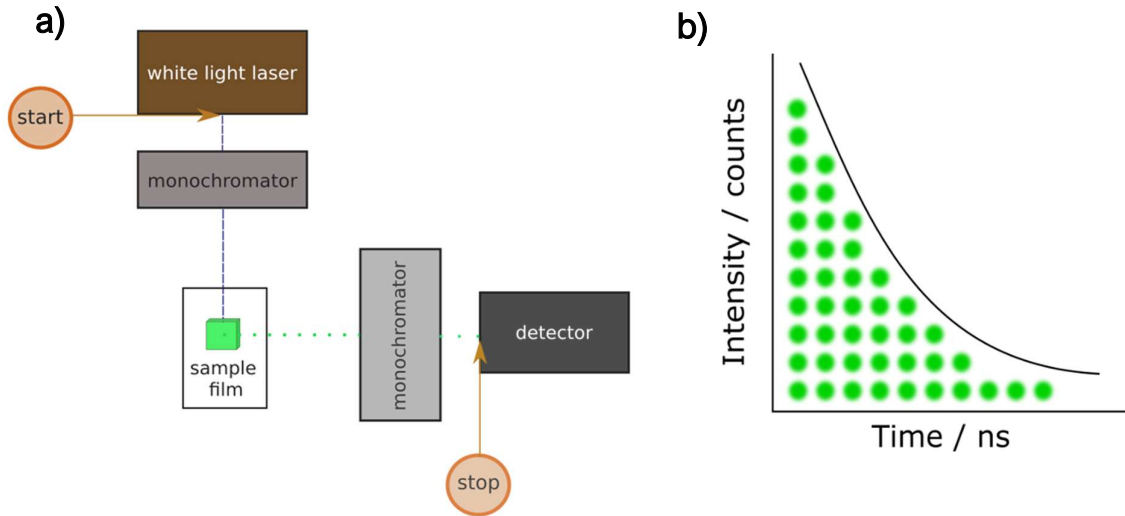
Figure 2. a) Simplified scheme of the TCSPC set-up and **b)** obtained histogram with reconstructed PL decay curve.

From this histogram of single photon counts, the photoluminescence decay curve of the investigated material can be reconstructed. It is also important to note, that the detector has a certain dead time after a photon has been detected. In this time, photons that are later hitting the detector will not be detected. Since only the information of the first detected photon is processed, a high rate of fluorescence photon counts on the detector would lead to a pile-up of early photon counts and therefore the decay curve will be falsely constructed. In order to preserve a low probability of more than one photon hitting the detector, the photon count rate at the detector is adjusted to a value that corresponds to approximately 1 % of the repetition rate of the laser[2].

The fluorescence lifetime of materials is strongly dependent on sample parameters (e.g. chemical composition, solvent, dispersant) as well as measurement parameters (e.g. temperature, excitation light fluence). By varying different sample and measurement parameters, the dependence of the lifetime can be examined. The elucidation of these dependencies can reveal essential information to understand the nature of the excited states of the sample and their relaxation mechanisms as well as the influence of sample parameters on the excited states[2].

1.2. Perovskite nanoparticles

Organic-inorganic hybrid halide perovskites are a prominent class of perovskite materials with advantageous optical and electronic properties, such as tunable band gap energy, high absorption coefficient, high charge carrier mobility and defect tolerance[3]. Organic-inorganic hybrid halide perovskite materials are defined by their characteristic ABX_3 crystal structure, which is shown in **Figure 3**. Thereby, A corresponds to a monovalent organic cation (e.g. methylammonium), B to a divalent cation (e.g. Pb^{2+}) and X to a halide anion[4]. The divalent cations (B) form a complex with the halide anions (X) resulting in an arrangement of corner-sharing octahedra[4]. Moreover, the cations (A) are positioned in the space between the ions that form the octahedral structure, and thereby are neutralizing the present charge of the complex[4]. If the composition of the perovskite material is altered, the band gap of the structure will also be affected[5]. Consequently, the optical properties of such perovskites can be influenced[5]. Nanomaterials of these perovskites can be prepared by techniques such as the hot-injection method or the ligand-assisted reprecipitation method[6]. In both cases organic capping ligands are utilized which passivate the surface of the perovskite core and stabilize the nanocrystalline state[6]. In this work the nanoparticles based on the perovskite materials formamidinium lead bromide ($FAPbBr_3$) and methylammonium lead bromide ($MAPbBr_3$) were used. Nanoparticles were fabricated using the ligand-assisted reprecipitation method, employing N_α-(*tert.*-butyloxycarbonyl)-L-lysine and hexanoic acid as capping ligands. The fabricated perovskite nanoparticles are additionally surrounded by a matrix material of unknown composition[7].
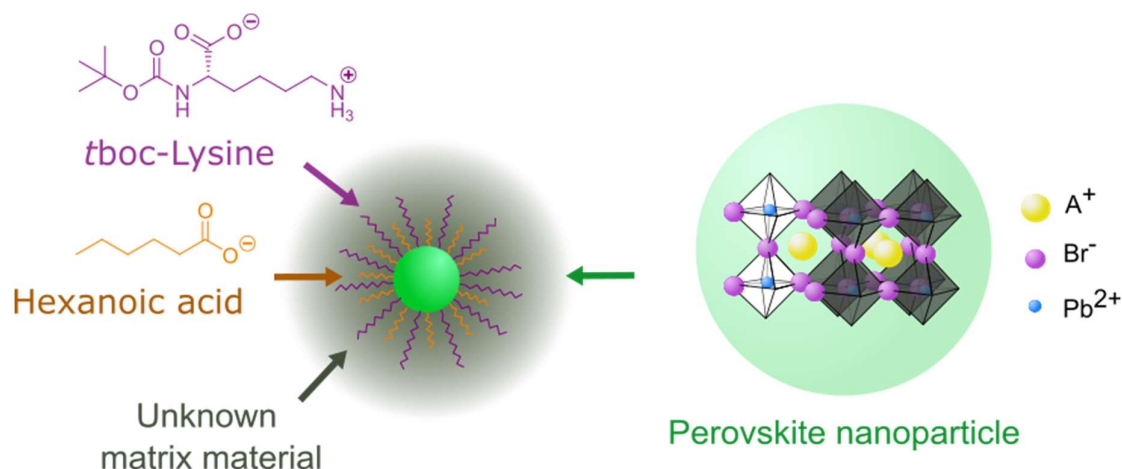
Figure 3. Organic-inorganic hybrid halide lead perovskite structure with capping ligands adapted from reference [8].

1.3. Encapsulation of PNPs in polymer matrices

Lead-halide perovskite particles have been reported to show low stability against moisture[9]. To reduce the effects of humidity on the luminescence stability of PNPs, the embedment of PNPs into a shielding polymeric matrix has been proposed by Raino *et al.*[10]. Important for an efficient embedment of the PNPs is the interaction between polymer and passivating ligand in terms of polarity[10]. The hydrophobic polystyrene serves as promising embedding material for highly hydrophobic PNP passivating ligands (e.g. oleic acid and oleylamine) leading to better optical properties in comparison with more hydrophilic polymers[10,11]. Additionally, if a sufficient interaction of polymer and PNPs exists, a fine and homogenous distribution of particles in the polymer matrix can be achieved[10]. This is not only important for the reduction of sensitivity against moisture, but also allows studies on the optical properties of single-particle emitters[12]. Furthermore, PL lifetimes show to be correlated with the degree of passivation of traps states[13]. It was observed that better passivation leads to longer PL lifetime since trap-assisted non-radiative recombination induces a fast early decay component[13].

Another crucial property that has an influence on the optical behaviour of PNPs is their size and size distribution. As described by Crooker *et al.*[14], the PL lifetime in a nanocrystal ensemble is linked to the inter-particle energy transfer occurring after excitation. It has been shown that smaller nanoparticles, which show a higher energy PL, can transfer energy to larger particles upon photoexcitation. This serves as a fast alternative relaxation pathway besides radiative recombination and leads to a steep decrease in PL intensity (fast decay component) during the first nanoseconds of the PL decay function when observing the PL at the high-energy side of the ensemble emission spectrum. On the other hand, when higher wavelengths are used for excitation primarily larger NPs which show lower energy PL are excited. As the probability that those big NPs find even larger PNPs to transfer their energy to is low, the energy transfer occurs less frequently, and the energy is released via a radiative decay. This radiative excited state decay is much slower compared to the decay curve involving the fast energy transfer of small particles. Consequently, the PL decay curve measured at lower emission energies related to the larger nanoparticles is less steep and the PL lifetime increases for excitation on the low energy side. By embedding PNPs in a finely distributed manner into a polymeric matrix, the PNPs are separated from each other. Thereby, the distance between two neighboring particles is increased by decreasing the concentration of PNPs in the polymer. As a results, the described energy transfer at excitation with higher energies might be hindered and the fast decay component at high-energy side of the PL is supposed to vanish to some extent. Consequently, the PL lifetime should increase for higher degrees of dilution[14].

In this work, the aim is to finely distribute PNPs in a sample thin film by embedding the PNPs into a transparent polymer matrix. In order to achieve this goal, a suitable polymer has to be found that is compatible with the investigated PNPs. Importantly, also different treatment methods are investigated to separate PNP agglomerations which hinder the accomplishment of a fine PNP distribution (see **Figure 4**).
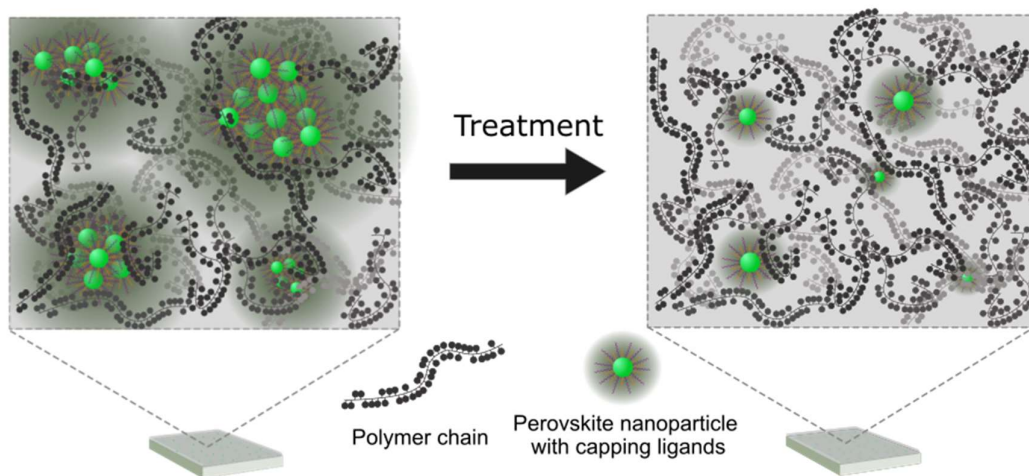
Figure 4. PNP clusters embedded in a polymeric matrix and single PNPs after treatment.

2. <u>Experimental</u>

2.1. Sample Preparation

2.1.1. Perovskite Nanoparticle Dispersions

The perovskite particles used in this study were prepared by DI Felix Mayr (Johannes Kepler University Linz, Austria) and by Elisabeth Leeb, BSc (Johannes Kepler University Linz, Austria). The synthesis was conducted following the procedure described by Leeb E.[8]. Thereby, the perovskite nanoparticles (PNPs) were produced by precipitation upon injection of 150 µL precursor solution in DMF, containing the ligands *t*-boc-Lysine (*t*-boc-lys) and hexanoic acid (HeA), into toluene. A controlled crystal growth and size of the PNPs could be achieved by the addition of a specific amount of water to the precursor solution. From the dispersion in toluene, the obtained nanoparticles were centrifuged at 5000 rpm for 5 min. The supernatant was discarded and the produced PNPs were redispersed in 2 mL of toluene using the ultrasound bath producing a PNP concentration of approximately 1 mg mL^{-1}. The 2 mL colloidal PNP solution were then further used for the experiments. Standard synthesis parameters like the perovskite composition and ligands are listed in **Table 1**.

Table 1. Synthesis parameter of the PNPs films.

No. of sample	perovskite composition	ligand	molar ratio of water[1]
1	$MAPbBr_3$	*t*-boc-lys/HeA	32 equiv.
2	$FAPbBr_3$	*t*-boc-lys/HeA	16 equiv.

[1] with respect to $PbBr_2$ in the precursor solution

2.1.2. Solvent test

Different solvents ranging from polar to non-polar were first tested as dispersion medium for the $MAPbBr_3$ and $FAPbBr_3$ particles. The tested solvents were H_2O, methanol (MeOH), ethanol (EtOH), 2-propanol (i-PrOH), acetonitrile (ACN), dimethyl sulfoxide (DMSO), chloroform, ethyl acetate, dichloromethane (DCM), tetrahydrofuran (THF), diethyl ether (Et$_2$O) and toluene. For the tests, 100 µL of the PNP stock dispersion are added to 1 mL of the tested solvents. The photoluminescence of the dispersions was then examined after 1 h and 24 h under illumination of UV light at 254 nm.

2.1.3. Polymer solubility test

Following from the solvent test acetonitrile, DCM, THF, diethyl ether and toluene were selected for further investigation. In order to find a polymer that is suitable for embedding the perovskite nanoparticles, first the solubility of the six polymers polystyrene (PS), polymethyl methacrylate

(PMMA), polyethylene glycol (PEG), polyvinyl pyrrolidone (PVP), polyvinyl alcohol (PVOH) and polyvinylidene fluoride (PVDF) in the selected solvents was examined. For the solubility test approx. 10-20 mg of the respective polymer were dispersed in 1 mL of the respective solvent (ACN, DCM, THF, Et$_2$O and toluene). If the polymer was not fully dissolved at room temperature, the dispersion was heated up and/or treated with ultrasound.

2.1.4. Polymer-PNP compatibility test

The stability of the investigated PNPs in solutions of the polymers listed in section 2.1.3 were investigated. For this purpose, 40 µL original PNP dispersion were added to 100 µL of 20 mg mL^{-1} polymer-solvent solution. The mixtures were treated with ultrasound for approx. 30 s. Afterwards, the PL of the dispersed PNPs was examined under radiation of UV-light at 254 nm.

Further embedding studies were carried out with ca. 20 mg mL^{-1} solutions of the following polymers:

- PS in toluene, THF or DCM
- PMMA in toluene, THF or DCM
- PVDF in THF or DCM

2.1.5. Preparation of pristine PNP films, concentrated and diluted PNP-polymer films

Pristine PNP films were prepared by dropcast deposition from the respective PNP dispersions onto glass substrates (1x1 cm^2) which were pre-treated with an oxygen plasma for 5 min at 100 W. Depositions were carried out at room temperature.

For the preparation of the concentrated PNP-polymer films, 40 µL of the approx. 20 mg mL^{-1} polymer solution were added to 200 µL of the original PNP dispersions. Thereby, the same solvent was used as PNP dispersant as well as solvent for polymer dissolution. The mixture was then treated with ultrasound for approx. 30 s and afterwards drop-casted onto a glass substrate (1x1 cm^2) that was pre-treated with oxygen plasma for 5 min at 100 W.

In order to prepare the diluted PNP-polymer films, the stock PNP dispersion was diluted 1:5, 1:10, 1:20, 1:50 and 1:100 with the respective polymer solution (approx. 20 mg mL^{-1}), whereby again the dispersant and the polymer solvent were matching. The diluted PNP-polymer dispersions was treated with ultrasound for approx. 30 s. Afterwards, the mixture was immediately spin coated at room temperature onto a glass substrate (13x13 mm^2) that was pre-treated using oxygen plasma (5 min, 100 W). Here, standard spin coating parameters were used, which are listed in **Table 2**.

Table 2. Standard spin coating parameter used for all experiments.

	time / s	rpm / min^{-1}	ramp / rpm s^{-1}
1	30	800	400
2	20	4000	1000

It is important to note, that although special attention was paid to the dilution and spin coating step, exact concentrations of PNPs on the films cannot be provided. The reason for this problem was that a portion of the PNPs were sticking to the glass walls of the vials as well as to the pipette tip. This could not be hindered by sonication before spincoating the dilutions onto the glass substrate.

2.1.6. Dispersion, washing and sonication experiment

For redispersion of the PNPs in different solvents, the 1.5 mL of the original PNP dispersions were put into a centrifugation vial and placed into a centrifuge for 5 minutes at 5000 rpm. The supernatant was discarded and the sedimented PNPs were redispersed in 1.5 mL of new solvent (THF or DCM) using an ultrasonic bath. For the dispersion experiment, the dispersion was filled into a vial and further used for making pristine PNP films, concentrated as well as diluted PNP-polymer films after 2 h and 24 h following the standard procedure described in section 2.1.5.

For the PNP solvent washing, the same procedure was performed except that after 20 min the dispersion with new solvent (THF or DCM) was centrifuged again for 5 minutes at 5000 rpm. Subsequently, the supernatant was discarded and the PNPs were redispersed in 1.5 mL toluene. The washed dispersion was then further used in the standard procedure for making pristine PNP films, concentrated as well as diluted PNP-polymer films.

The sonication experiment was performed by adding 1 mL of toluene to 500 µL of the original dispersion. Then, this mixture was treated with ultrasonic processor (Hielscher UP50h, 50 W, Cycle: 1, amplitude: 100 %) for 0 s, 30 s, 2 min and 10 min under cooling on an ice bath. The ultrasonicated dispersion were used to fabricate concentrated PNP-PS films as well as PNP-PS films in the concentrations of 1:10 and 1:100 following the standard procedure.

2.2. Sample Characterization

2.2.1. Time-correlated single photon counting measurements

The time-correlated single photon counting (TCSPC) measurements under different measurement temperatures were conducted using a custom-made setup. The investigated sample was mounted on a copper sample holder inside a closed-cycle helium cryostat (Oxford Instruments Optistat Dry) equipped with a temperature controller (Oxford Instruments Mercury iTC). The cryostat sample chamber was put under vacuum (ca. 10^{-6} hPa) by a turbomolecular pump (Pfeiffer Vacuum). A supercontinuum white light laser (NKT Photonics SuperK extreme FIU-15) was used as a radiation source connected to the monochromator (Photonetc LLTF contrast). With this combination not only a specific wavelength can be selected from the broad range of wavelengths (400 – 1000 nm) with high spectral brightness, but also the maximum power output can be regulated between 15-100%. For the experiments the laser was operated at a repetition rate of 3.12, 4.34 and 4.88 MHz depending on the measured PL lifetime. The output light beam was then guided into the sample chamber by an assembly of two mirrors and focussed onto the center of the mounted sample film. Light emitted by the excited sample was then collimated by a lens (plano-convex, focal length f = 50 mm). An iris diaphragm was put into the set-up to adjust the amount of emitted light passing through. This diaphragm is followed by a mirror that guides the light to two focus lenses (Thorlabs LA1433 plano-convex, focal length f = 150.0 mm and Thorlabs LA1608 plano-convex, f = 75.0 mm) which focus the emission light onto the monochromator entrance slit. Two suitable longpass filters were placed in front of the monochromator slit to ensure a sufficient attenuation of the excitation wavelength in the recorded spectrum. Using a monochromator (DeltaNu DNS-300, grating: 600 l/mm, 500 nm blaze; slit: 1 mm) a specific emission wavelength was selected and the incoming photons were detected with the photomultiplier tube (Becker & Hickel PMC-100-1). The instrument response function has a full width half maximum of approx. 230 ps, as seen in
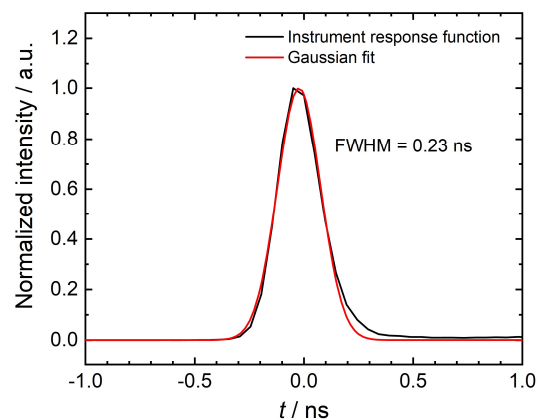
Figure 5. Instrument response function with Gaussian fit (red).

Figure 5. Since the response function was much shorter than the typically measured PL decay times, no correction of the decay function was applied.

For the investigated PNP films, measurements of the PL decay were performed at temperatures of 4, 100, 200 and 295 K. For a thorough characterization, measurements under variation of the detected emission wavelength were performed at each temperature. Prior to these measurements, the steady-state emission spectrum of the PNP film was recorded at each respective temperature (see Low-Temperature Photoluminescence spectroscopy). Since the lower wavelength tails of the steady-state emission spectra of the investigated films extended to wavelengths down to ca. 460 nm, the excitation laser wavelength was set to 415 nm for the TCSPC measurements at different emission wavelengths. This excitation wavelength was chosen due to the comparatively high laser power at this wavelength which allows to easily reach a sufficient emission intensity of the sample. Consequently, a 435 nm and a 455 nm longpass filter were used in the emission light path to block the excitation laser light. Besides measuring at the emission maximum, the PL decay curves were recorded at two emission wavelengths below and above the PL maximum. For all measurements the excitation power of the laser was held constant in order to eliminate any possible impact on the PL lifetime. Additionally, the respective integration time was adjusted according to the detected number of photons.

2.2.2. Temperature dependent steady-state photoluminescence measurements

Temperature dependent steady-state photoluminescence spectra were recorded using a custom-made set-up. Measurements were performed on PNP samples mounted in the closed cycle helium cryostat as described in section 2.2.1. A 405 nm continuous wave laser (Coherent OBIS) was used as excitation source. The laser light was guided to the sample chamber and the emitted light of the sample is coupled into an optical fiber by a fiberport equipped with a lens. A set of lenses is placed in front of the output fiberport which focus the light on the aperture of an Andor Shamrock monochromator (grating 2: 300 l mm^{-1}; blaze: 760 nm) equipped with an Andor iStar (iCCD) detector (cooled to -30°C). Two 420 nm optical longpass filters are placed in front of the aperture to block the 405 nm excitation light. Measurements were carried out at the temperatures described in 2.2.2.

2.2.3. PLQY measurements at room temperature

Photoluminescence quantum yield (PLQY) measurements were carried out by a. Univ.-Prof. Dr. Markus Scharber. The measurements were performed on a Hamamatsu Photonics quantum yield measurement system, which was equipped with a Xe lamp, an A10080-01

monochromator, an A9924-06 integrating sphere and a PMA-12 multichannel analyser. All measurements were performed at an excitation wavelength of 405 nm.

2.2.4. Magnetic field measurements at low temperature

The study of magnetic field effects on the photoluminescence of perovskite PNPs was performed in a magneto-optical measurement system. Thereby, the Physical Property Measurement System (PPMS) Dynacool type (Quantum Design) was used which was equipped with a single-stage pulse tube cooler. In this way, measurements in a temperature range from 1.8 K to 400 K could be carried out. Using an electromagnet, a magnetic field strength of up to ± 9 T could be applied onto the sample inserted into the PPMS. An OBIS 405 nm laser diode was used for excitation and the emitted light was focused onto the slit of the Andor Shamrock monochromator (grating 2: 300 l mm^{-1}; blaze: 760 nm) equipped with an Andor iStar (iCCD) detector (cooled to -30°C). Excitation and emission light were coupled in/out of the PPMS sample chamber by optical fibers. A more detailed description of the used setup is provided by Putz C.[15].

For the investigated PNP films first PL spectra were recorded at temperatures of 4 K, 50 K, 100 K, 125 K, 200 K, and 295 K. For a thorough examination of the magnetic field effects, the PL spectra were recorded several times at a magnetic field strength of 0 T, 1 T, 3 T, 5 T and ±9 T at a fixed temperature of 4 K.

2.2.5. Optical microscopy

For optical microscopy an Eclipse LV100ND – Nikon was used in bright field and fluorescence mode.

High-resolution fluorescence microscopy was carried out on a Nikon Eclipse 150LV microscope equipped with a Nikon L-UEPI illuminator with a 100 W halogen lamp and a dark-field condenser. A 100x objective (Nikon, NA 0.90) was used. For the fluorescence microscopy the microscope was operated in dark-field mode and a 525 nm optical short-pass filter was placed in front of the halogen lamp. To detect only the PL of the investigated PNPs, a 550 nm longpass filter was placed in the detection channel of the microscope.

3. Results and Discussion

3.1. Effect of different solvents on PNP dispersions

In course of this study different polymers are investigated as polymeric matrix for embedding perovskite nanoparticles in a finely dispersed and homogenised manner. For this, solvents have to be determined that are compatible with the perovskite particles and that could properly dissolve the tested polymers. Additionally, it was previously observed that the synthesized PNPs, especially $FAPbBr_3$ PNPs, show an increased tendency of cluster and aggregate formation in toluene. In these dispersions, large particle aggregates are visible to the naked eye and the aggregation phenomenon results in a fast sedimentation of the PNPs. This strong agglomerate formation is attributed to the presence of a matrix material around the PNPs synthesized by the procedure used in this study[7]. This occurrence of PNP clusters is unfavourable for preparing a fine distribution of PNPs in a polymer matrix. In order to investigate the effect of solvent choice on cluster formation and emission colour of PNPs, different solvents ranging from polar to non-polar were first tested as dispersion medium for the $MAPbBr_3$ and $FAPbBr_3$ particles. The PNP stability and aggregation tendency in each investigated solvent were qualitatively investigated by observing the PNP photoluminescence under UV light illumination (254 nm) and the PNP sedimentation behaviour. The results are listed in **Table 3**.

Table 3. Compatibility of tested solvents for $MAPbBr_3$ and $FAPbBr_3$ PNPs.

	#	solvent	$MAPbBr_3$	$FAPbBr_3$
polar	1	H_2O	X	X
	2	MeOH	X	X
	3	EtOH	X	X
	4	i-PrOH	X	X
	5	ACN	✓	✓
	6	DMSO	X	X
	7	$CHCl_3$	~	~
	8	Ethyl acetate	✓ (agglomeration↑)	✓ (agglomeration ↑)
	9	DCM	✓ (agglomeration ↓)	✓ (agglomeration ↓)
	10	THF	✓ (agglomeration ↓↓)	✓ (agglomeration ↓↓)
non-polar	11	Et_2O	✓	✓
	12	Toluene	✓	✓

As seen in **Table 3**, polar solvents like H_2O and ethanol (EtOH) proved to be non-suitable as dispersant due to PNP degradation, whereas the PNPs in most of the less polar solvents still emit light under illumination with UV-light at 254 nm. The use of acetonitrile (ACN), chloroform ($CHCl_3$), dichloromethane (DCM) and tetrahydrofuran (THF) resulted in a visible blue-shift of the emission light with the strongest blue-shift observed in THF. The dispersions in chloroform additionally showed a relatively fast decrease in the emission intensity of dispersed particles over time while dispersions in ACN showed a much slower decrease of emission intensity with time. Dispersions in DCM and THF still showed stable bright light emission. In contrast to this, ethyl acetate and diethyl ether (Et_2O) exhibited a green light emission that was similar to that of the original toluene dispersion. **Figure 6** shows an exemplary depiction of the PNPs dispersed in the solvents 5-12 (see **Table 3**) illuminated with UV-light, whereby the emission light colours of the respective dispersant only slightly varied for all conducted dispersant tests. The PNPs in ethyl acetate showed increased aggregation compared to the original toluene dispersion. In contrast to this, for THF a clear, stable cluster-free dispersion was obtained, where also no particle sedimentation was observed after 24 h. A similar observation was made for ACN and DCM, whereas here still PNPs agglomeration and sedimentation were visible. For Et_2O as dispersant no change in aggregation tendency could be seen compared to the original toluene dispersion.

Subsequently, acetonitrile, dichloromethane, tetrahydrofuran, diethyl ether and toluene were selected for further experimental use. Using them as dispersion medium showed either a visible reduction in PNP aggregation size or the intensity of fluorescence remained unchanged decreased compared to the original dispersion using toluene**.**
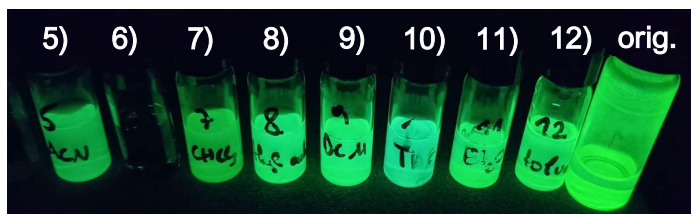
Figure 6. PNPs dispersed in different solvents: **5)** ACN, **6)** DMSO, **7)** $CHCl_3$, **8)** ethyl acetate, **9)** DCM, **10)** THF, **11)** Et_2O, **12)** toluene and the original dispersion under illumination with UV light at 254 nm.

3.2. Solubility of polymers in selected solvents

In order to find a polymer that is suitable for embedding perovskite nanoparticles, first the solubility of the six polymers polystyrene (PS), polymethyl methacrylate (PMMA), polyethylene glycol (PEG), polyvinyl pyrrolidone (PVP), polyvinylalcohol (PVOH) and polyvinylidene fluoride (PVDF) in the selected solvents had to be examined. The selection of used solvents is based on the compatibility of the solvents with the PNPs (see Effect of different solvents on PNP

dispersions). The obtained results are presented in **Table 4**, whereby insoluble and soluble is marked as X and ✓, respectively.

Table 4. Solubility of different polymers in the selected solvents.

	solvent	PS	PMMA	PVDF	PVP	PEG	PVOH
polar	**ACN**	X	✓	X	✓	✓	X
	DCM	✓	✓	✓	✓	✓	X
	THF	✓	✓	~	✓ at 45°C	✓ at 45°C	X
	Et₂O	X	X	X	X	X	X
non-polar	**toluene**	✓	✓	X	X	X	X

It could be observed that diethyl ether (Et$_2$O) did not dissolve the tested polymers even upon treatment with ultrasound. Therefore, Et$_2$O was excluded from further investigations. Furthermore, it could be seen that none of the selected solvents could dissolve PVOH, which was also not further tested.

3.3. Compatibility of PNPs with polymer materials

The solubility test was followed by checking the compatibility of PNPs and the polymers, which were both dispersed in the same solvents (ACN, DCM, THF, toluene) (see **Table 5**). For this test, FAPbBr$_3$ PNP dispersions in the investigated solvents were added to polymer solutions in the same solvent and the PL of the resulting mixtures was qualitatively investigated under UV irradiation. All PNP dispersions that still were emitting light under illumination of UV-light were marked as ✓. When the fluorescence of the dispersion vanished, the mixture was labelled as X. For solvent-polymer combinations in which the PNPs showed stable photoluminescence, solid PNP-polymer films were fabricated and investigated under UV radiation. As shown in **Table 5**, the compatibility of PNPs in ACN was not given for the tested polymers PMMA, PVP and PEG. Moreover, all dispersions using DCM appeared to emit light under UV radiation. For THF all dispersions except with PVP were emitting light. In both cases, however, solid films of PNPs embedded in PVP and PEG did not show any light emission under UV illumination anymore. PNPs dispersed in toluene proved to be compatible with PS and PMMA. The presented results were obtained for FAPbBr$_3$ PNPs and due to the typically similar behaviour in comparison to MAPbBr$_3$ it was assumed that the found results are also valid for MAPbBr$_3$ PNPs. Due to the obtained compatibility results, the further investigation was focussed on the use of toluene, THF and DCM as solvents and PS, PMMA and PVDF as polymer matrices.

Table 5. Compatibility of polymers with PNPs dispersed in the respective solvent.

	solvent	PS	PMMA	PVDF	PVP	PEG
PNPs dispersed in	acetonitrile	-	X	-	X	X
	DCM	✓	✓	✓	~*	~*
	THF	✓	✓	✓	X	~*
	toluene	✓	✓	-	-	-

* Dispersion was still fluorescent but solid PNP-polymer films did not emit light under radiation of UV-light.

3.4. Dispersion of PNPs in THF and DCM

Followed by a general check of compatibility, further examinations concerning the embedding of PNPs into polymer were conducted. Prior to this, it is important to distinguish between influence of polymers and solvents, especially THF and DCM, on the PNPs. For this purpose, the impact of THF and DCM on the PNPs was examined in more detail by redispersion of the PNPs in THF and DCM, respectively and fabrication of pristine PNP films from these dispersions after 2 h and 24 h. The PLQY and PL maximum wavelengths of the corresponding FAPbBr$_3$ PNP films in comparison to those prepared from the initial dispersions in toluene are summarized in **Table 6**. Additionally, also MAPbBr$_3$ PNP were examined, but here the PNPs were only dispersed in THF and DCM for 2 h. The corresponding results are shown in **Table 7**.

Generally, it could be observed for FAPbBr$_3$ PNPs that the PLQY of particles dispersed in THF and DCM decreased with time while the PLQY values of toluene films remained similar. The films fabricated from PNP dispersions in DCM showed a moderate decrease of PLQY and shift to higher emission wavelengths over time. In contrast, the films fabricated from THF showed a strong red-shift of emission and significant decrease of PLQY already after 2 h of dispersion of the PNPs in THF. Interestingly, for both THF and DCM a clearly visible blue-shift of the PNP PL in the dispersion as compared to toluene could be observed under UV illumination while the corresponding pristine PNP films fabricated from the dispersions in THF and DCM showed emission at higher wavelengths than those deposited from toluene (see **Figure 7**).
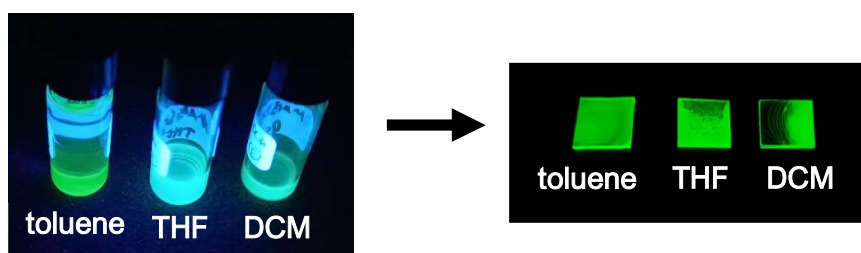
Figure 7. Dispersion of PNPs in toluene, THF and DCM (left side) and dropcast pristine PNP films (right side) from the corresponding dispersions under UV light illumination at 254 nm.

This behaviour was not observed for the PNP dispersions in toluene. A possible explanation for this observation could be a solvent-PNP interaction in the case of THF and DCM. These more polar solvents could potentially dissolve the matrix material around the PNPs (see 3.1. Effect of different solvents on PNP dispersions) and the capping ligands, depending on the residence time in the solvent. This could lead to a decrease in degree of surface passivation and lower PLQY in the pristine PNP films with increasing dispersion time in the respective solvent. Simultaneously, the solvent molecules might interact with PNPs and to a certain extent passivate the PNPs in the dispersions. This leads to a bright-blue-shifted emission which is indicative of the presence of smaller PNP sizes. The emission might shift to longer wavelengths in the solid PNP films again, due to evaporation of the solvent and PNPs again agglomerate forming clusters during the drying process. It should be noted, however, that over the course of the study, different batches of $FAPbBr_3$ and $MAPbBr_3$ PNPs were investigated which showed slight differences in the degree of passivation and initial PLQY values. These PNP specific properties slightly influence the behaviour of PNPs towards different dispersion solvents. Additionally, the water content in THF might have been changing leading to varied measured values. Thus, no consistent relative decrease of PLQY and shift of emission wavelength could be determined.

Table 6. Dependence of PLQY and the maximum emission wavelength of dropcast pristine PNP films on the dispersion duration in the respective solvent.

No. of sample	perovskite composition	dispersant	dispersion time / h	PLQY / %	em λ_{max} / nm
1	$FAPbBr_3$	toluene	2	100	527
2	$FAPbBr_3$	toluene	24	100	527
3	$FAPbBr_3$	THF	2	53	542
4	$FAPbBr_3$	THF	24	40	543
5	$FAPbBr_3$	DCM	2	93	530
6	$FAPbBr_3$	DCM	24	88	535

Table 7. Dependence of PLQY and the maximum emission wavelength of dropcast pristine PNP films on the dispersion duration on the respective solvent.

No. of sample	perovskite composition	dispersant	dispersion time / h	PLQY / %	em λ_{max} / nm
1	$MAPbBr_3$	toluene	2	98	513
2	$MAPbBr_3$	THF	2	97	513
3	$MAPbBr_3$	DCM	2	91	514

3.5. Polymer embedment of PNPs

After checking the solvent and polymer compatibilities of the investigated PNPs, studies on the embedding of MAPbBr$_3$ and FAPbBr$_3$ nanoparticles in PS, PMMA and PVDF were conducted. Hence, PNP dispersions with a selected polymer were made and subsequently, concentrated and diluted films were prepared (see 2.1.5. Preparation of pristine PNP films, concentrated and diluted PNP-polymer films). As obtaining a fine and homogenous particle distribution plays a key role in this study, the diluted PNP-polymer films were investigated by bright-field and fluorescence microscopy.

Figure 8 shows a comparison of a PNP:PS-THF and a PNP:PS-DCM film. Here, it can be clearly seen that for both films using PS clusters were formed in the polymeric matrix. Additionally, the films showed bubble inclusions and a rough and inhomogeneous surface Similar morphologies were also observed for the combinations PNP:PMMA-DCM and PNP:PMMA-THF.
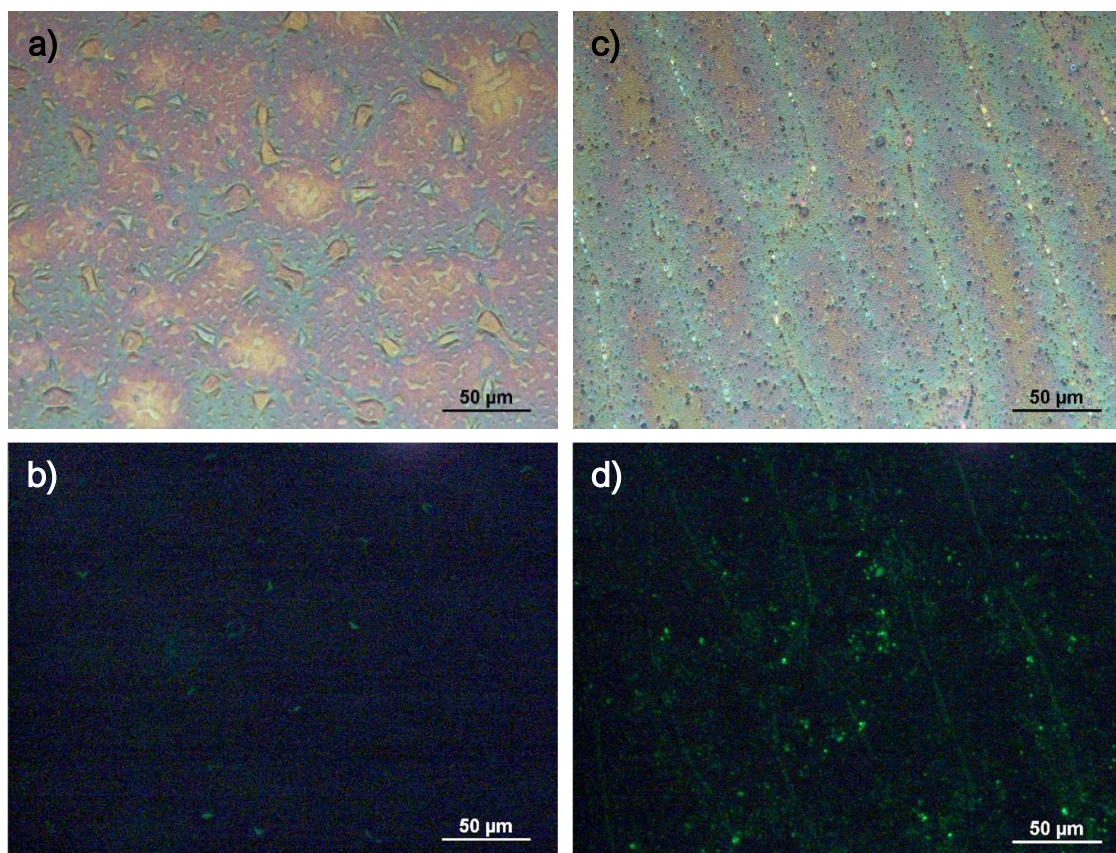
Figure 8. Microscope pictures (magnification: 40x) of **a)** FAPbBr$_3$ PNP:PS-THF and **c)** FAPbBr$_3$ PNP:PS-DCM films in bright-field mode both with a volumetric ratio of 1:10, whereby **b)** and **d)** show the same spots on the thin films investigated in fluorescence mode, respectively.

In contrast to THF and DCM, PNP:PS and PNP:PMMA films fabricated from toluene showed a smooth and homogeneous surface and a better distribution of the embedded PNP, however the nanoparticles still showed strong cluster formation (see **Figure 9**). Since PNP dispersed in toluene are reported to achieve high PLQY values[8] and are stably storable, the focus was put on PS-toluene and PMMA-toluene for further investigations.
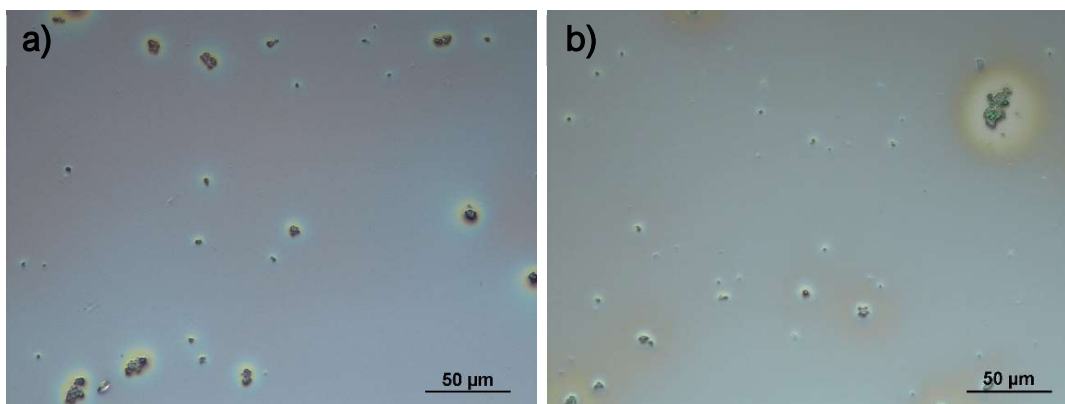
Figure 9. Microscope pictures (magnification: 40x) of **a)** FAPbBr$_3$ PNP:PS-toluene and **b)** FAPbBr$_3$ PNP**:**PMMA-toluene films (volumetric ratio 10:1).

Furthermore, PVDF was used as polymeric matrix for THF-PNP and DCM-PNP dispersions. In **Figure 10** PVDF polymer islands are shown in which the PNPs are finely distributed without larger particle agglomerations. A reason for this advantageous interaction between the PNPs and PVDF might be the large binding capacity of PVDF for amino acids[16]. PVDF might interact with the passivating ligands t-boc lysine and thereby distribute the PNPs more finely compared to the other polymers dissolved in THF and DCM (see **Figure 8**). This might lead to a decreased PNP cluster formation in the film.
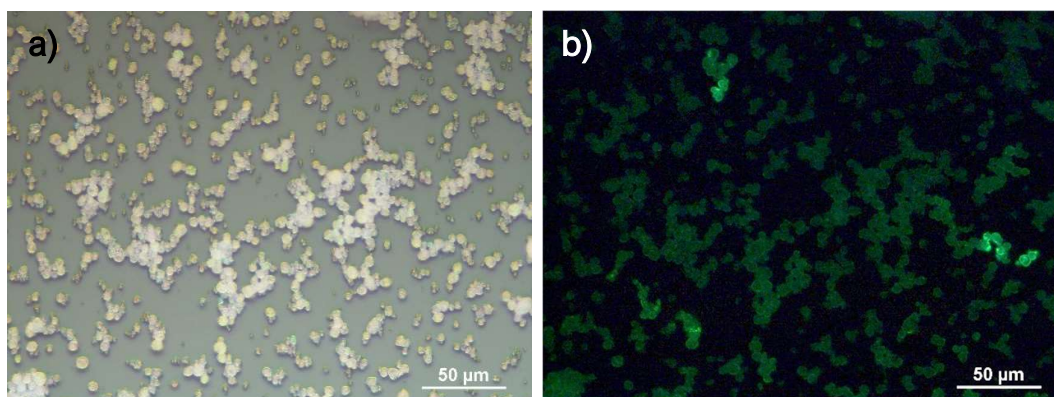
Figure 10. Microscope pictures (magnification: 40x) of **a)** a FAPbBr$_3$ PNP:PVDF-DCM film (volumetric ratio 10:1), whereby **b)** show the same spots on the thin films investigated in fluorescence mode, respectively.

To study the influence of the polymer matrix on the PLQY and the emission maximum of the embedded PNPs, concentrated PNP-polymer films (ratio: 5:1) were made. In **Table 8** and **Table 9** one can see the PLQY and maximum emission wavelength of several combination of polymers and used dispersion solvent. The respective films were dropcasted after the PNPs were dispersed in the new solvent for 48 h (see **Figure 11**).

It could be observed that the PS and PMMA had no influence on the optical parameter of the PNPs dispersed in toluene. Additionally, the PLQY values for the PNP:PS-toluene thin film remained constant over 1 week. This suggest that the PNPs can be properly protected against ambient influences by the proper embedding into PS.
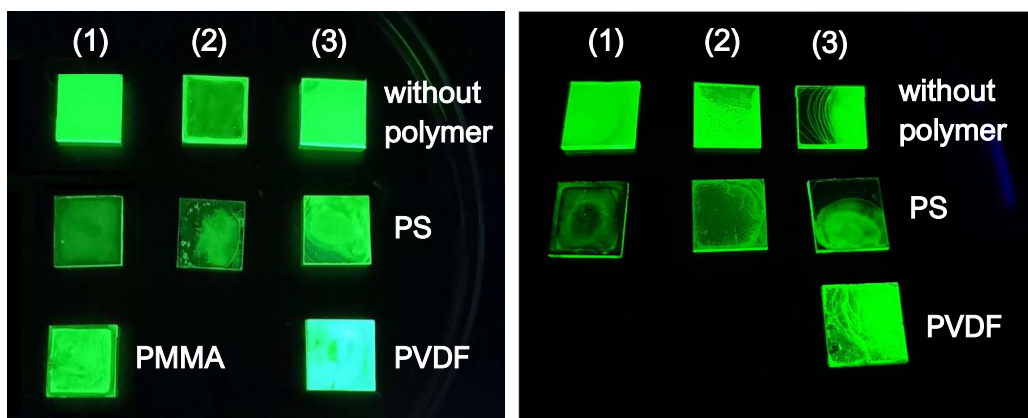
Figure 11. FAPbBr$_3$ (left) and MAPbBr$_3$ (right) PNPs dispersed in 1) toluene and 2) THF and 3) DCM embedded in the polymers PS, PMMA and PVDF shown under illumination with UV light at 254 nm.

Table 8. Results of pristine PNP and concentrated PNP-polymer films fabricated from dispersions of FAPbBr$_3$ in toluene, THF and DCM.

No. of sample	perovskite composition	dispersant	Polymer	PLQY / %	em λ_{max} / nm
1	FAPbBr$_3$	toluene	-	98	529
2	FAPbBr$_3$	toluene	PS	97	527
3	FAPbBr$_3$	toluene	PMMA	99	530
4	FAPbBr$_3$	THF	-	53	542
5	FAPbBr$_3$	THF	PS	43	532
6	FAPbBr$_3$	DCM	-	93	530
7	FAPbBr$_3$	DCM	PS	65	535
8	FAPbBr$_3$	DCM	PVDF	80	532

Table 9. Results of pristine PNP and concentrated PNP-polymer films fabricated from dispersions of MAPbBr$_3$ in toluene, THF and DCM.

No. of sample	perovskite composition	dispersant	Polymer	PLQY / %	em λ_{max} / nm
1	MAPbBr$_3$	toluene	-	98	513
2	MAPbBr$_3$	toluene	PS	95	511
3	MAPbBr$_3$	THF	-	97	513
4	MAPbBr$_3$	THF	PS	94	513
5	MAPbBr$_3$	DCM	-	91	514
6	MAPbBr$_3$	DCM	PS	81	520
7	MAPbBr$_3$	DCM	PVDF	90	513

Furthermore, the results of the experiments show that PVDF gives a similar or even higher PLQY values for both THF- and DCM-dispersed PNPs as compared to PS or PMMA. Consequently, PVDF shows the potential of stabilizing PNPs after the removal of the matrix surrounding the PNPs. Additionally, the fluorescence microscopy images suggest a nice distribution of PNPs in diluted PNP-polymer films without the presence of larger cluster agglomeration. It is important to note here, that the surface of PVDF is rather uneven forming polymer islands, when PVDF is processed in ambient conditions. This rough surface leads to problems during characterization of the polymer films. Smoother PVDF films could be prepared when deposited in a nitrogen-filled glovebox as proposed by Li *et al.* [17]. However, in course of this study the focus was not put on the optimization of PVDF films and for this reason PVDF was only processed in air.

In general, PNPs dispersed in DCM or THF showed significantly lower PLQY values than PNPs dispersed in toluene. As a consequence, the focus was put only on the PNP-polymer combinations PNP:PS-toluene and PNP:PMMA-toluene in this work. As for these combinations an increased PNP cluster formation was observed within the polymers, a treatment method has to be found for decreasing the PNP cluster size. In this way, a fine distribution of PNPs in PS or PMMA might be realizable.

3.6. Effect of sonicating on cluster size

In course of this study, PS and PMMA show a promising embedding behaviour for PNPs dispersed in toluene. Although still cluster formation of PNPs was observed which is unfavourable for a homogeneously distributed PNP-polymer film. As a consequence, ultrasonication was investigated as a potential method of cluster size reduction. For this purpose, a dispersion of MAPbBr$_3$ PNPs was ultrasonicated for durations of 0.5 to 10 min and the sonicated dispersions were immediately used for fabrication of pristine PNP films and

PNP-polymer films with different PNP concentrations. **Table 10** presents typical PLQY and emission wavelength values for pristine PNP films obtained from the ultrasonication experiments.

Table 10. Results of pristine MAPbBr$_3$ PNP films made in a sonicating experiment.

No. of sample	perovskite composition	solvent	sonication time / min	PLQY / %	em λ$_{max}$ / nm
1	MAPbBr$_3$	toluene	0	87	520
2	MAPbBr$_3$	toluene	0.5	86	517
3	MAPbBr$_3$	toluene	2	80	518
4	MAPbBr$_3$	toluene	10	59	515

The data gathered from several sonicating experiments show, the PLQY values and the maximum emission wavelength of the investigated PNPs were not significantly changed upon sonication treatment for 0-2 min. However, longer sonicating treatment led to an unfavourable decrease in PLQY values. Additionally, fluorescence microscope pictures revealed that the tendency of cluster formation was not decreased. Fluorescence microscope pictures of diluted PNP-polymer films, which were treated for 10 min showed that the size of clusters increased and the formation of additional PNP agglomerations might be promoted.

3.7. Reduction of cluster size by washing with selected solvents

As shown in chapter 3.3, the properties of PNPs dispersed in THF and DCM for 2 h visibly changed in terms of agglomeration tendency, sedimentation behaviour of the PNPs and emission colour. While the investigation of the dispersions in THF and DCM suggested a significant decrease of particle agglomeration, an unfavourable decrease of PLQY and shift of emission wavelength was observed. To avoid this unwanted change of PL properties but still benefit from the decrease of the agglomeration tendency of the PNPs, washing of the PNPs with THF and DCM with only short contact time of PNPs with the solvent was investigated. In this way, the PNP could possibly be finely dispersed in the solvent and the initial high-quality PL properties of the PNPs originally dispersed in toluene could be retained. Consequently, washing the PNPs with THF and DCM before the encapsulation in a polymer was examined for the potential as cluster size reduction method. For this purpose, the PNPs were redispersed in THF or DCM from the original toluene dispersion and after 20 min redispersed in toluene again. The washed PNP redispersions in toluene were used for the preparation of pristine PNP and PNP-polymer films with different concentrations.

When comparing bright-field microscope images of THF/DCM washed FAPbBr$_3$ PNP:PS films fabricated from a dilution of PNP dispersion with 20 mg mL^{-1} PS solution in a volumetric ratio of 1:10, the size of the clusters could significantly be reduced by washing with THF (see **Figure 12**). In contrast to this, washing with DCM has only slightly changed the PNP agglomeration size. Consequently, the focus was put onto the washing procedure with THF. In order to further investigate if not only large PNP clusters were scaled down by the washing with THF but also single particles were separated, high-resolution fluorescence microscope pictures were taken of MAPbBr$_3$ PNP:PS films (volumetric ratio 1:5). These small-scale microscope images prove that using the washing procedure the visible PNPs clusters could be significantly reduced in size to approx. 700 nm (see **Figure 13 b)**) and the likelihood of even smaller agglomerations being present is increased. Hence, the smaller clusters might approach a single-emitter behaviour that could be further characterized.
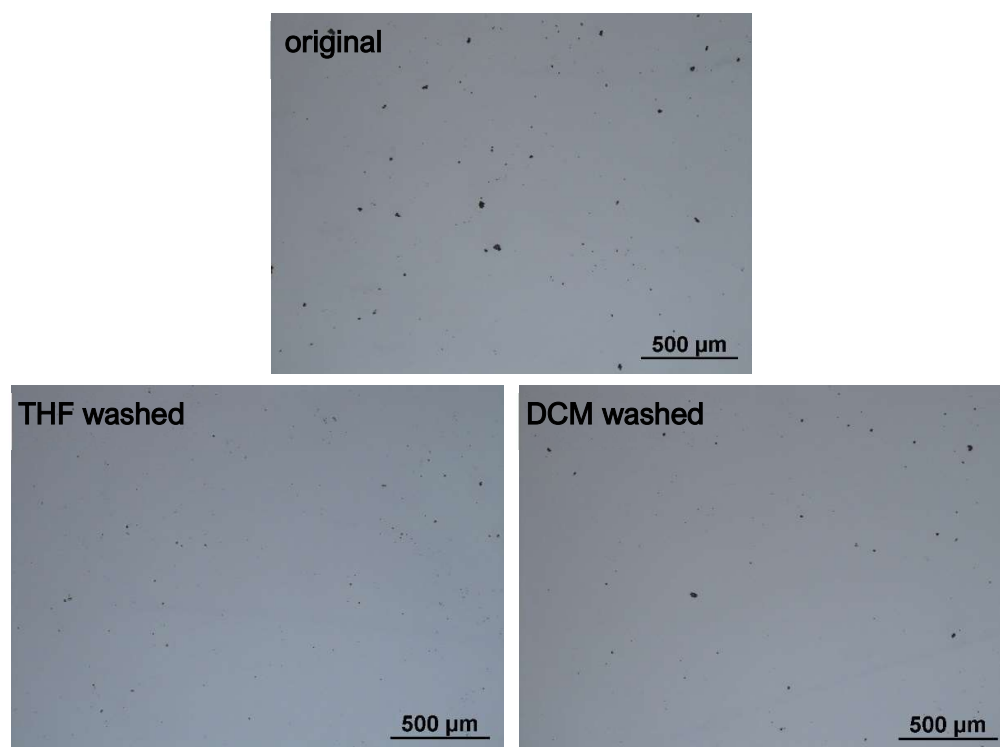

Figure 12. Bright field pictures of FAPbBr$_3$ PNP:PS films (volumetric ratio 1:10) whereby particles were embedded without washing, and with washing with THF and DCM before embedment, respectively.
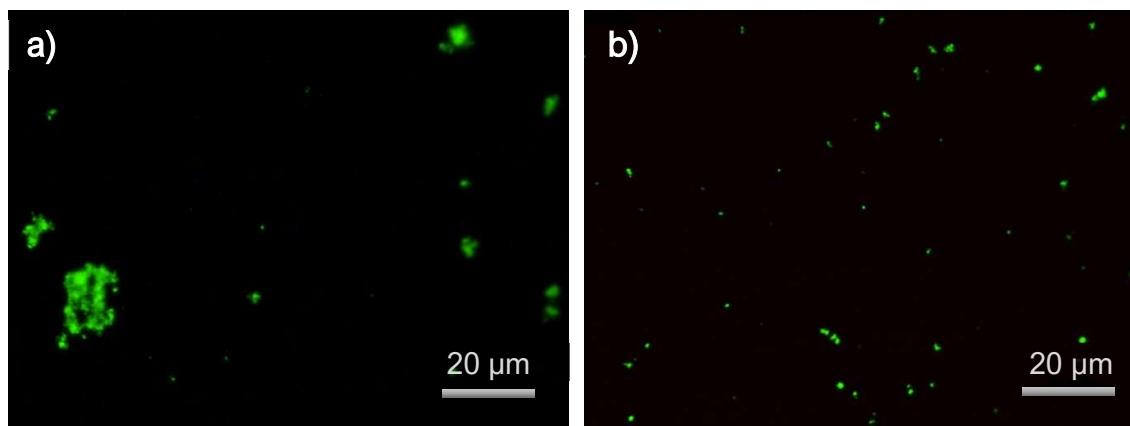
Figure 13. MAPbBr$_3$ PNP:PS films (volumetric ratio 1:5) films investigated in fluorescence mode whereby, **a)** PNPs were embedded without washing and **b)** PNPs were washed with THF before embedment.

Next, concentrated PNP-PS films were made in order to establish the influence of the washing procedure on the PNP PL properties. The PLQY values and the maximum emission wavelengths of PNP-PS film fabricated from untreated as well as the corresponding THF washed PNPs can be found in **Table 11**. **Figure 14** shows the corresponding concentrated films under illumination with UV-light.

Table 11. Results of pristine PNP and concentrated PNP-polymer films fabricated from dispersions made of unwashed and THF washed PNPs.

perovskite composition	solvent	Polymer	PLQY / %	PLQY / % after 7 days	em λ$_{max}$ / nm
MAPbBr$_3$	toluene	-	98	-	523
MAPbBr$_3$	toluene	PS	86	-	523
MAPbBr$_3$	toluene	PMMA	88	-	522
MAPbBr$_3$	toluene (THF washed)	-	72	-	522
MAPbBr$_3$	toluene (THF washed)	PS	84	-	522
MAPbBr$_3$	toluene (THF washed)	PMMA	89	-	523
FAPbBr$_3$	toluene	-	89	84	535
FAPbBr$_3$	toluene	PS	84	85	533
FAPbBr$_3$	toluene	PMMA	88	-	533
FAPbBr$_3$	toluene (THF washed)	-	86	79	534
FAPbBr$_3$	toluene (THF washed)	PS	88	86	532
FAPbBr$_3$	toluene (THF washed)	PMMA	89	-	532

Figure 14. Pristine PNP films and concentrated polymer films fabricated from untreated and THF washed FAPbBr$_3$ and MAPbBr$_3$ PNPs shown under illumination with UV light at 254 nm.

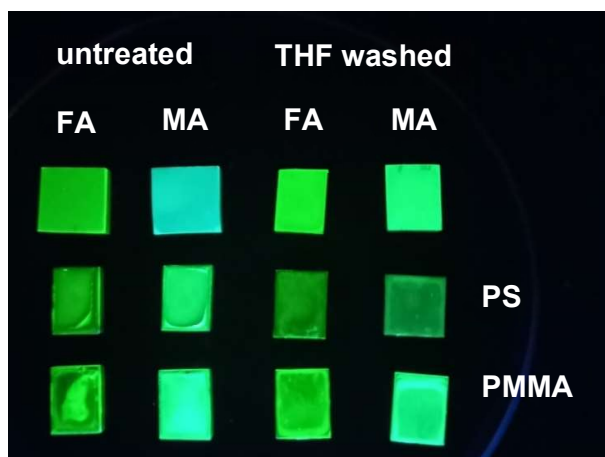Compared to the properties of the untreated PNPs the PLQY values of the pristine THF washed PNP films slightly decreased whereas the corresponding emission wavelengths remained similar for both FAPbBr$_3$ and MAPbBr$_3$ PNPs. Interestingly, for THF washed PNPs embedded into a polymer (PS or PMMA) PLQY values were acquired that match the values of untreated PNPs. Moreover, the PLQY values of the both untreated and treated FAPbBr$_3$ PNP-PS films did not change when being measured after 7 days. In contrast to this, the pristine PNP films especially the ones using THF washed PNPs showed decreased PLQY values. This suggests, that the PNPs could be protected from ambient influences that could cause aging effects and damage to their high-quality initial properties.

3.8. Low-Temperature Photoluminescence spectroscopy

For this work low-temperature photoluminescence measurements were conducted in order to examine if the THF washing procedure has somehow influenced the PNPs with respect to their photoluminescence emission spectra. In this chapter, untreated and THF washed PNPs are compared according to their PL emission spectra, the PL temperature dependence and the relation of emission spectra to the PNP concentration within a PNP-polymer film.

3.8.1. Temperature dependence of PL emission spectra

In general, the peak shape of PL emission spectra is primarily affected by electron-hole pair (exciton) recombination. Beside this, the particle size distribution, trap states and exciton-phonon interactions are also contributing to the PL emission appearance[5].

In course of the low temperature PL measurements the same trend could be observed for all sample films including unwashed and THF washed PNP-polymer films in all orders of dilution. An exemplary PL spectrum of one concentrated and one diluted PNP-polymer film measured at different temperatures is shown in **Figure 15**. The inset presented in **Figure 15** shows the integrated PL intensity and the FWHM of the PL spectra measured at the respective temperature.
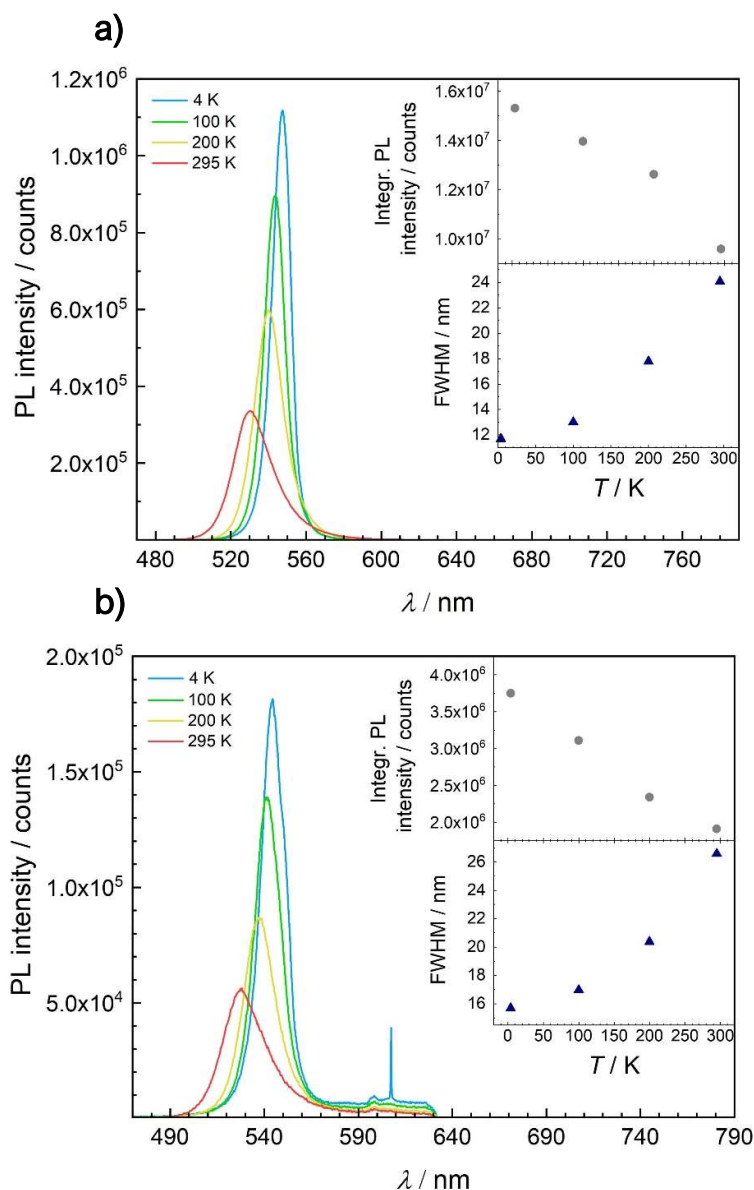

Figure 15. PL emission spectra measured at different temperatures temperature-dependent photoluminescence spectra, the corresponding integrated PL intensity as well as the full width at half maximum (FWHM) of THF washed FAPbBr$_3$ PNPs embedded into PS in **a)** a volumetric ratio of 5:1 and **b)** 1:10. The spectra were recorded at an excitation wavelength of 405 nm.

For all measurements, it was observed that for increasing temperature, the emission maxima shifted towards lower wavelength (blue shift), which can be seen exemplarily in **Figure 15**. Additionally, the full-width half maximum increased toward higher temperature while the integrated PL intensity decreased from 4 K to 295 K. These trends were measured for all PNP-polymer sample films. The observed decrease in integrated PL intensity is mainly explainable by the presence of trap states and surface traps in PNP-polymer films. At higher temperature those traps states more strongly interact with the excitons and therefore have a greater influence on the PL intensity at higher temperatures, which is also known as thermal quenching[18].

For all PNP films the symmetry of the PL peak increased with decreasing temperature. In **Figure 15 a)** one can see a shoulder at higher wavelength for all temperatures but observed only for diluted PNP-PS films (1:5,1:10,1:20). This effect might be attributed to the fluorescent behaviour of glass that has a maximum emission wavelength of approx. 600 nm. As for higher order of dilution the PL intensity decreases the glass fluorescence is more dominant than for more concentrated films.

It is important to note that the band gap energy E_g of conventional semiconductors typically decreases upon a temperature increase due to enhanced electron-phonon interactions and thermal expansion of the crystal lattice. Consequently, a red shift of emission spectra is observed for most semiconductors[19]. In contrast to this, bulk perovskite films are reported to show a rather unusual shift of PL towards the lower wavelength regions upon increasing the temperature[20]. This blue shift could be explained by the thermally induced expansion of the crystal lattice leading to a change in potential energy of the valence band maxima and the conduction band minima. Here, the interaction of the two valence orbitals is reduced and therefore the band gap energy is increased[21]. However, the full explanation of the temperature dependent shift is still heavily under discussion and therefore further research is necessary.

3.8.2. Comparison of PL emission spectra of untreated and THF washed PNP-polymer films

Previous research has indicated an observed blue shift in PL spectra for small CdSe quantum dots (QD) compared to larger CdSe QDs[22]. In this study, the PL emission spectra of THF washed and unwashed PNPs showed a similar effect, whereby the THF washed PNPs appear to be present in smaller PNP cluster sizes compared to the unwashed PNPs (see **Figure 16**). Additionally, the PL emission spectra of THF washed PNPs exhibits a larger full width half maximum (FWHM) compared to the PL spectra of unwashed PNPs. This difference in FWHM might be explained by THF washed PNPs having a larger PNP size distribution. Another

possible explanation for this effect could be that due to the THF interaction the energy transfer from small to bigger PNPs is hindered and consequently, the spectrum gets broader at the high energy side.
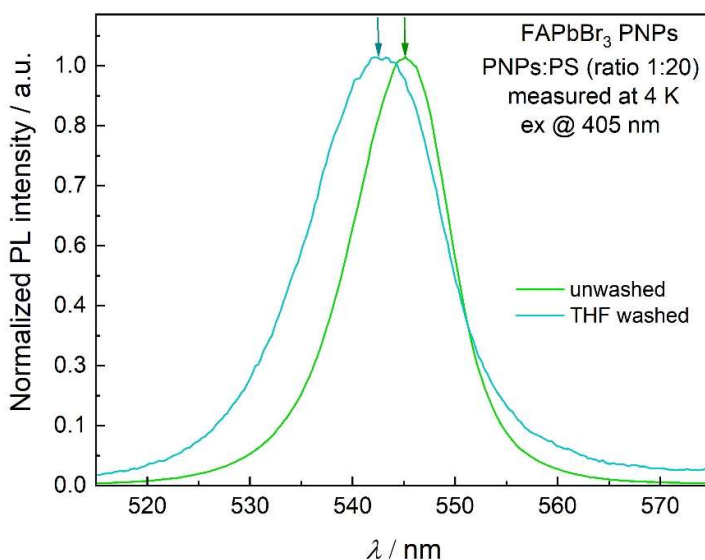

Figure 16. PL emission spectra measured at 4 K of unwashed and THF washed PNPs embedded into PS in a volumetric ratio of 1:20. The arrows are pointing to the respective emission maxima.

3.8.3. Influence of PNP concentration on PL emission spectra

In **Figure 17** the PL spectra of THF washed and unwashed PNPs embedded into PS at different volumetric ratios are illustrated. As clearly visible in **Figure 17**, with increasing concentrations of PNPs (THF washed and unwashed) in the polymer the PL spectrum shows an increasing red-shift. This concentration dependent spectral red-shift also known as inner filter effect (IFE) is well-studied for solution PL measurements but less researched for solid-film samples[23]. Considering sample dispersions, this effect originates from the concentration dependent change of the dielectric constant of the surrounding of the PNPs as well as the Förster Resonance Energy Transfer (FRET)[23]. For solid-state dispersions Koc *et al.*[23] reported that highly concentrated quantum dot (QD) films involving QD clusters show PL spectra which are red-shifted compared to spectra of diluted solid film samples. The authors attribute this phenomenon to increased FRET interactions in QD clusters, which are not observed for isolated QDs in dilute solid-state dispersions. For PNP clusters a similar behaviour could be expected which can account for the red-shift observed at higher PNP concentrations. Since this red-shift was observed for both the THF washed as well as the unwashed PNP films, this trend could be most likely attributed to a photon reabsorption of the emission of smaller PNPs by larger PNPs or PNP agglomerations leading to higher wavelength emission or further FRET interactions before the photons are emitted.[23]
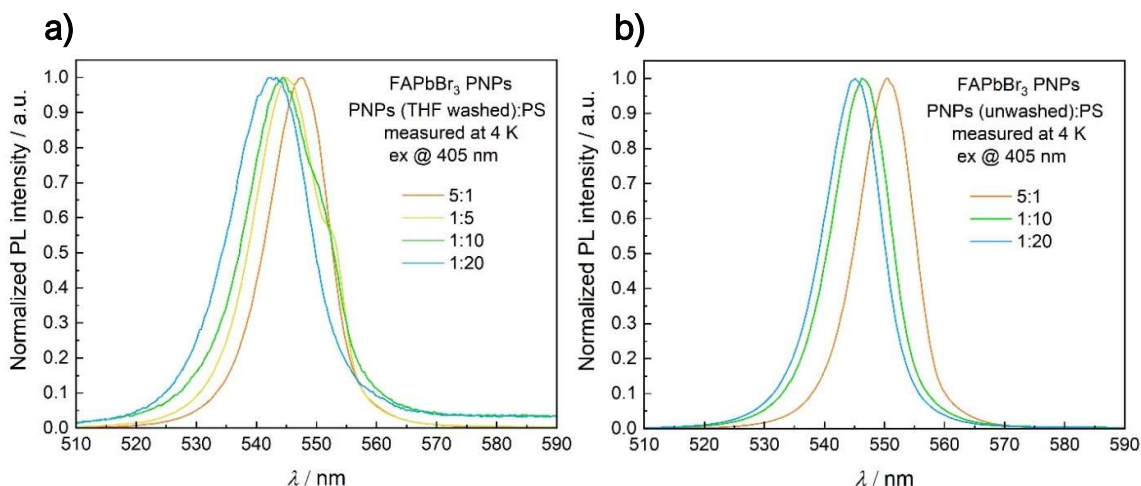
Figure 17. PL emission spectra measured at 4 K of **a)** THF washed and **b)** unwashed PNPs embedded into PS in different volumetric ratios.

3.9. Time-correlated single photon counting measurements

3.9.1. Influence of emission wavelength on PL lifetime of PNP-polymer films

After the examination of steady-state PL emission spectra, time-resolved measurements were conducted in order to investigate if the unwashed and THF washed PNPs embedded into a polymer show any difference in dependence of the PL lifetime on the emission wavelength. **Figure 18** displays an exemplary depiction of the PL decay curves obtained from the TCSPC measurements of THF washed and unwashed PNPs.

Figure 18. Comparison of the PL decay curves of FAPbBr$_3$ PNP:PS (1:20) films at different emission wavelengths with excitation @ 415 nm measured at 4 K. – The emission maximum (marked bold) of **(a)** sample film using THF washed PNPs lies at 543 nm and for **(b)** the unwashed PNPs at 545 nm.

Figure 18 shows the comparison of PL decay curves of two sample films using **(a)** THF washed PNPs and **(b)** unwashed PNPs, respectively. The PL decay curves were measured at different emission wavelengths at 4 K, whereby the emission maximum is marked bold in the legend of the graph. In general, it was observed that when going from the lowest measured emission wavelength to the emission maximum the PL lifetime increases. This trend was measured for both unwashed and THF washed PNP:PS sample films for all orders of dilution and at every measured temperature. When measured at 4 K a slight increase in PL lifetime for emission wavelengths above the maximum was observed. Additionally, the PL decay curves for all selected emission wavelengths of every sample exhibit two decay components: a fast and a slow decay component, as seen in **Figure 18 a)** and **b)**. Considering measurements at higher temperatures, the decay curves show both a fast and a slow decay component at lower emission wavelengths measured for all orders of dilutions (see **Figure 19**). At the PL maximum and above it only the slow component appears to be present. Moreover, for PL decay curves measured at 295 K the shape of PL decay curves measured above the emission maximum do not change significantly. Therefore it is assumed that also the PL lifetime remains the same.
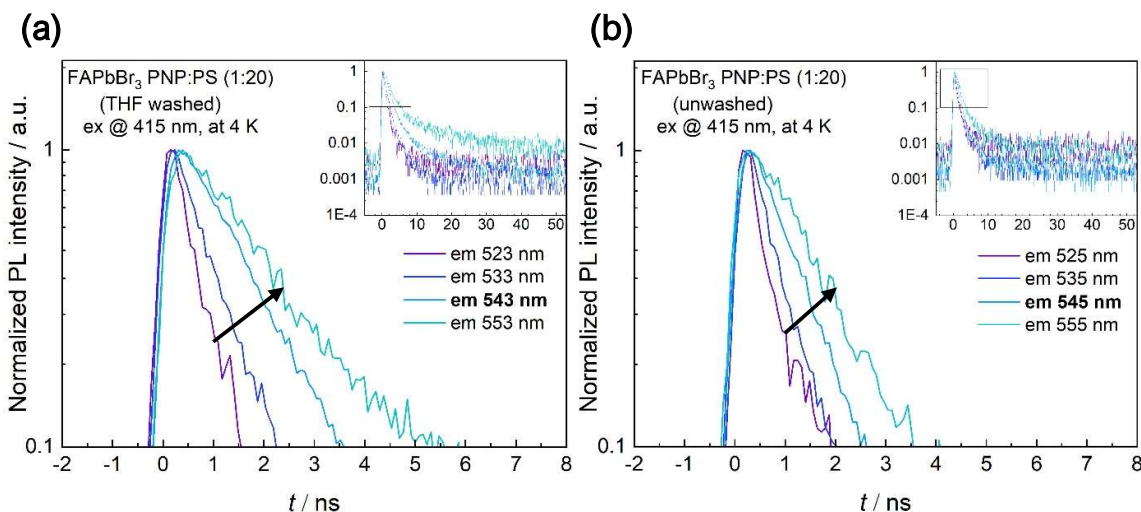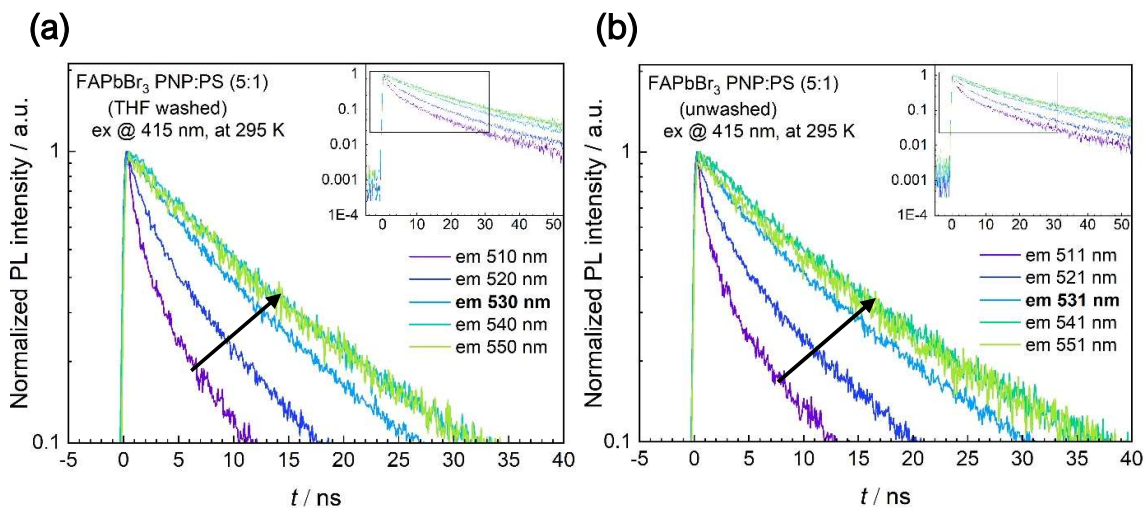

Figure 19. Comparison of the PL decay curves of FAPbBr₃ PNP:PS (5:1) films at different emission wavelengths with excitation @ 415 nm measured at 295 K. – The emission maximum (marked bold) of **(a)** sample film using THF washed PNPs lies at 530 nm and for **(b)** the unwashed PNPs at 531 nm.

3.9.2. Dependence of PL lifetime on PNP concentration within a PNP-polymer film

To study the dependence of PL lifetime on the PNP concentration within a polymer film it is assumed that the size PNP agglomerates could be sufficiently reduced by the THF washing procedure. In this respect, the PNP-polymer films are considered to show a sufficiently fine and homogenous distribution of PNPs utilizable for further PNP concentration dependence studies.

When measuring at 4 K with an emission at 10 nm below the maximum wavelength, the PL lifetime slightly increases for THF washed PNPs with rising order of dilution (see **Figure 20 a)**). A similar trend has been previously reported in literature[14]. It was stated that the PL lifetime showed a significant increase for decreasing PNP concentration. The reason for this effect might be that by increasing the order of dilution within a PNP-polymer film the average distance between two PNPs can be increased. Due to this increase in distance the possibility for an inter-particle energy transfer to happen is decreased. These energy transfers serve as a fast alternative relaxation pathway besides radiative recombination and lead to a steep decrease in PL intensity (fast decay component) during the first nanoseconds of the PL decay function when observing the PL at the high-energy side of the ensemble emission spectrum. If there is only a low tendency of energy transfers between the particles due to an increased distance, the PL intensity will decline slower. Consequently, higher values for the PL lifetime are obtained[14]. Even though for this work the same concentration dependence was seen, the observed trend was not as enhanced as it would be expected from literature[14]. Possibly, still smaller clusters are present in the sample films which would lead to a slightly reduced effect of the energy transfers. Consequently, the effect on the PL lifetime is more difficult to detect.
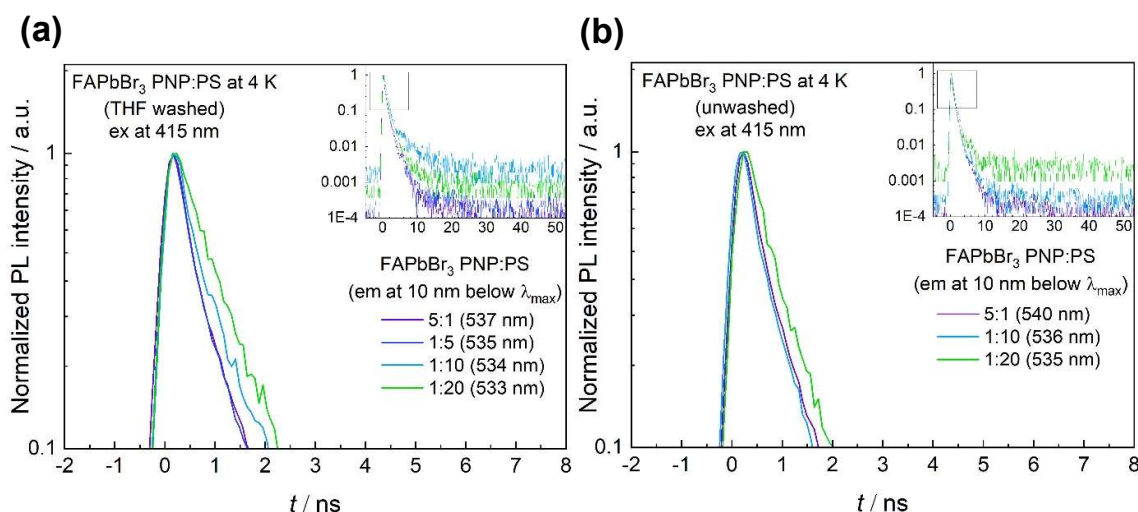

Figure 20. PL decay curves of differently diluted PNP-polymer films measured at the respective maximum emission wavelength - In **a)** the PNPs used for the fabrication of the PNP-polymer film were washed with THF and in **b)** the PNPs were used unwashed.

Another point which does not support the explanatory approach from literature[14] is that when measuring at 295 K no change in PL lifetime was seen for increasing the degree of dilution in the PNP-polymer films (see **Figure 21 a)**). According to Crooker *et al.*[14] the mentioned energy transfers should only depend on concentration rather than on temperature. Hence, an increase in PL lifetime should also be expected at 295 K. In contrast to this, the unwashed $FAPbBr_3$ PNPs-polymer films measured at the respective wavelength showed a similar PL lifetime for all concentrations at 4 K. In **Figure 20 b)** the PL decay curves of the unwashed PNP are presented, whereby the film with the voluemtric ratio 1:20 seems to show a longer PL lifetime compared to the other films. This observation might correspond to a slight displacement of the decay onset in the curve of the sample with a dilution of 1:20, while the PL decay time is similar to the more concentrated films. **Figure 21 b)** presents the PL decay curves measured at 295 K. Here, it can be clearly seen that the PL lifetime does not change for differently diluted PNP-polymer films. A possible explanation for this observation might be that untreated PNP:PS films showed a characteristic formation of PNP clusters for all volumetric ratios in contrast to the treated PNPs. Consequently, for these films only the concentration of clusters was changed, whereas the cluster size was unaltered throughout the sample films and the PNPs were still interacting due to their close vicinity. Hence, when measuring PNP-polymer films (unwashed) of different concentration, the laser beam hitting the films might has been fixed on a spot with higher density of PNP clusters. Consequently, similar PL lifetimes were obtained for different concentrated PNP:PS films by the measurements.
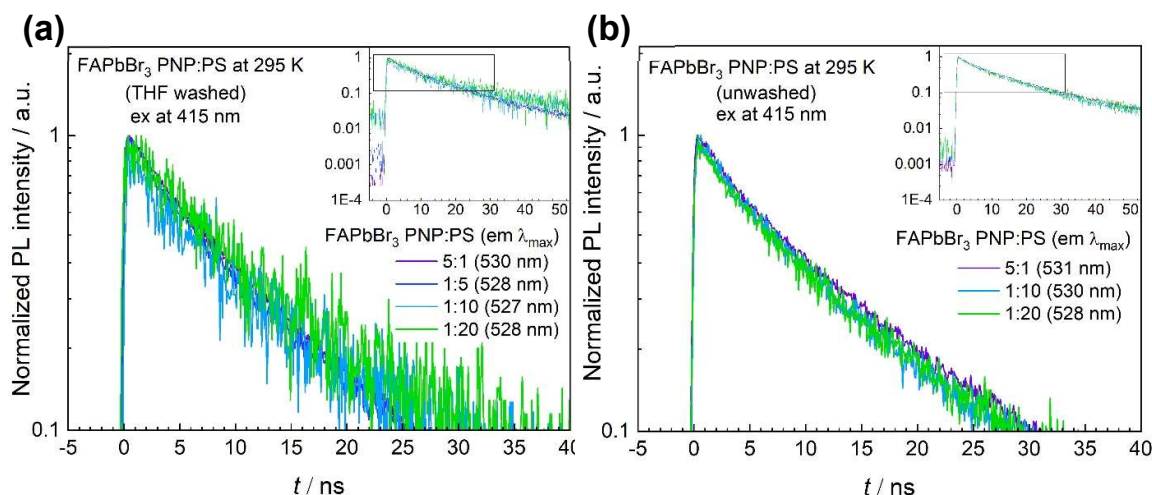

Figure 21. Comparison of the decay curves of $FAPbBr_3$ PNP:PS films with excitation @ 415 nm and PL measured at the respective emission maximum wavelength - **a)** the PNPs used were washed with THF and **b)** the PNPs were used unwashed.

3.10. Influence of magnetic field on PL intensity of finely distributed PNP thin films

In order to study the effect of the magnetic field on the PL intensity of the prepared diluted THF washed PNP-polymer thin films, measurements in a PPMS measurement system were conducted. The obtained PL spectra measured at 4 K and at different magnetic field strengths are shown in **Figure 21**. Interestingly, when applying a magnetic field of 9 T the PL intensity decreased by 3.8 % for the $FAPbBr_3$ PNP:PS (1:5, THF washed) film and 2 % for the $FAPbBr_3$ PNP:PS (1:10, THF washed) film, as seen in the insets of the respective graphs. A decrease of the PL intensity upon application of an external magnetic field has been reported by Pavliuk *et al.*[24] for $CsPbBr_3$ nanocrystal dispersions, although with a much stronger decrease in intensity of ca. 15 % and already at lower magnetic field strengths of 500 mT. The authors explained this decrease by a magnetic field dependent modulation of the triplet excited state population which act as non-radiative channels[24]. A similar decrease of PL intensity by ca. 1 % in a magnetic field of ca. 300 mT has been reported for bulk perovskite films by Hsiao *et al*[25]. They also attributed this decrease to suppression of the spin state mixing by the magnetic field which leads to an increase of the population of parallel spins in electron-hole pairs thus increasing the non-radiative triplet population[25]. As a consequence, the PL intensity is decreased[25].
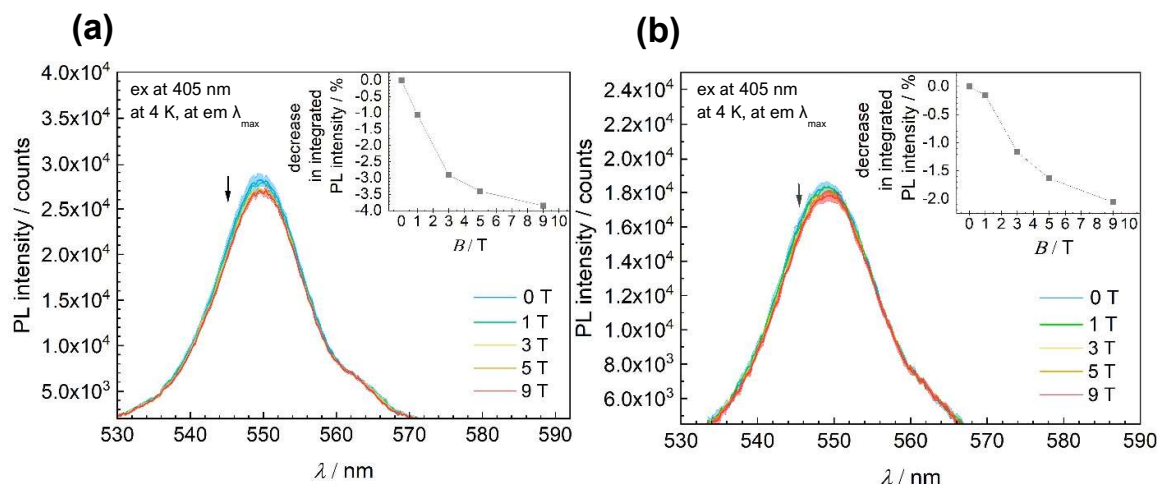

Figure 22. Averaged PL emission spectra measured several times at the respective magnetic field strength. The PL emission spectra correspond to **a)** a $FAPbBr_3$ PNP:PS film (THF washed, 1:5) and b) a $FAPbBr_3$ PNP:PS film (THF washed, 1:10). The inset in both panels shows the relative decrease of integrated PL intensity vs. the applied magnetic field strength.

4. Conclusion

The aim of this work was to distribute highly-fluorescent perovskite nanoparticles in homogenous and fine way in a polymeric matrix. It has been shown that the most promising PNP-polymer films in terms of compatibility and stability were prepared by PNPs dispersed in toluene embedded into polystyrene or polymethyl methacrylate. However, for this combination of PNPs, solvents and polymers a treatment method was necessary to reduce the size of PNP agglomerates before embedding the PNPs into the polymers. By washing the PNPs with THF the sizes of the PNP clusters could be visibly reduced without altering the PNP's original high-quality photoluminescence properties including PLQY and emission maximum. Additionally, the study showed that the untreated and THF washed PNPs exhibited similar trends concerning the temperature dependence of the PL emission spectra as well as the influence of the emission wavelength on the PL lifetime. The research has revealed that the PL lifetime of PNP-polymer films slightly increases with increasing order of dilution, whereby this effect was only observed for THF washed PNPs measured at low temperatures. Furthermore, it was found that the PL intensity of diluted PNP-polymer films using THF washed PNPs decreased by approx. 2-4 % when an external magnetic field was applied.

In course of this study a significant challenge were the fluctuating initial PLQY values of the PNP stock dispersions as well as their varying behaviour towards the solvents THF and DCM. Therefore, it would be highly recommended to further optimize the PNP synthesis procedure to obtain PNP batches with reproducible properties. Additionally, also the water content of the used solvents should be determined to ensure a reproducible PNP-solvent interaction. Even though in this study the size of PNP agglomeration could be significantly reduced, single nanoparticles could not be reliably separated. Therefore, it is highly recommended to do further research on the treatment method for PNP agglomerates.

Overall, PNP-polymer films show a promising distribution of PNPs in the polymeric matrices leading to highly interesting spectroscopic effects. These results suggest that the PNP-polymer films can be a basis to study the PL behaviour of single perovskite particles and besides this, the sample films show a great potential for the use in specific application, as for instance in LEDs.

5. Appendix

5.1. Chemicals

Table 12. List of solvents used in this study.

No.	Chemical	Abbreviation	M_w / g mol^{-1}	Purity	Supplier
1	Methanol	MeOH	32.04	ACS, Reag. Ph. Eur.	VWR
2	Ethanol	EtOH	46.07	ACS, Reag. Ph. Eur.	VWR
3	2-Propanol	i-PrOH	60.10	ACS, Reag. Ph. Eur.	VWR
4	Acetonitrile	ACN	41.05	≥ 99 %	VWR
5	Dimethyl sulfoxide	DMSO	78.13	≥ 99.5 %	Sigma-Aldrich
6	Chloroform	CHCl$_3$	119.38	99 %	VWR
7	Ethyl acetate	-	88.11	99.8 %	Sigma-Aldrich
8	Dichloromethane	DCM	84.93	≥ 99.8 %	Merck
9	Tetrahydrofuran	THF	72.11	ACS, Reag. Ph. Eur.	VWR
10	Diethyl ether	Et$_2$O	74.12	≥ 99.7 %	VWR
11	toluene	-	92.14	ACS, Reag. Ph. Eur.	VWR

Table 13. Polymer used in course of this study.

No.	Chemical	Abbreviation	Avg. M_w / g mol^{-1}	Supplier
1	Polystyrene	PS	350,000	Sigma-Aldrich
2	Poly(methylmethacrylate)	PMMA	15,000	Sigma-Aldrich
3	Polyethylene glycol	PEG	8,000	Sigma-Aldrich
4	Poly(vinylidene fluoride)	PVDF	534,000	Sigma-Aldrich
5	Poly(vinylpyrrolidone)	PVP	58,000	ACROS Organics
6	Poly(vinyl alcohol)	PVOH	89,000 – 98,000	Sigma-Aldrich

5.2. Further instruments

Table 14. Other instruments used.

No.	Instrument	Name and Supplier	Settings
1	Centrifuge	Hettich EBA 20	5 minutes at 50,000 rpm
2	Plasma Cleaner	PE-25 – Plasma Etch Inc.	equipped with a JB Industries Inc. DV-142N - Platinum 5 CFM vacuum pump, used with O$_2$ gas, at 100 W for 5 min
3	Ultrasonic processor	Hielscher UP50H	used with Hielscher MS1 UP50/100H (with cycle: 1 and amplitude: 100 %)
4	Ultrasonic bath	VWR Ultrasonic Cleaner	-

Literature

[1] PicoQuant, "Time-Resolved Photoluminescence (TRPL)", can be found under https://www.picoquant.com/applications/category/materials-science/time-resolved-photoluminescence.

[2] M. Wahl, "Time-Correlated Single Photon Counting", can be found under https://www.picoquant.com/images/uploads/page/files/7253/technote_tcspc.pdf, **2014**.

[3] Q. Chen, N. de Marco, Y. Yang, T.-B. Song, C.-C. Chen, H. Zhao, Z. Hong, H. Zhou, *Nano Today* **2015**, *10*, 355.

[4] P. Zolfaghari, G. A. de Wijs, R. A. de Groot, *Journal of physics. Condensed matter : an Institute of Physics journal* **2013**, *25*, 295502.

[5] S. Gholipour, M. Saliba in *Characterization Techniques for Perovskite Solar Cell Materials : Micro and Nano Technologies* (Eds.: M. Pazoki, A. Hagfeldt, T. Edvinsson), Elsevier, **2020**, pp. 1–22.

[6] E. V. Ushakova, S. A. Cherevkov, A. V. Sokolova, Y. Li, R. R. Azizov, M. A. Baranov, D. A. Kurdyukov, E. Yu Stovpiaga, V. G. Golubev, A. L. Rogach et al., *ChemNanoMat* **2020**, *6*, 1080.

[7] F. Mayr, E. Leeb, K. Matura, D. Ziss, O. Brüggemann, N. S. Sariciftci, Niyazi S., J. Hofinger, Y. Salinas, *submitted to ACS Appl. Nano Mater*.

[8] E. Leeb, *Bachelor Thesis*, Johannes Kepler Universität, Austria, **2020**.

[9] J. M. Frost, K. T. Butler, F. Brivio, C. H. Hendon, M. van Schilfgaarde, A. Walsh, *Nano letters* **2014**, *14*, 2584.

[10] G. Rainò, A. Landuyt, F. Krieg, C. Bernasconi, S. T. Ochsenbein, D. N. Dirin, M. I. Bodnarchuk, M. V. Kovalenko, *Nano letters* **2019**, *19*, 3648.

[11] S. N. Raja, Y. Bekenstein, M. A. Koc, S. Fischer, D. Zhang, L. Lin, R. O. Ritchie, P. Yang, A. P. Alivisatos, *ACS applied materials & interfaces* **2016**, *8*, 35523.

[12] D. K. Sharma, S. Hirata, M. Vacha, *Nature Communications* **2019**, *10*, 4499.

[13] S. B. Naghadeh, B. Luo, Y.-C. Pu, Z. Schwartz, W. R. Hollingsworth, S. A. Lindley, A. S. Brewer, A. L. Ayzner, J. Z. Zhang, *J. Phys. Chem. C* **2019**, *123*, 4610.

[14] S. A. Crooker, J. A. Hollingsworth, S. Tretiak, V. I. Klimov, *Physical review letters* **2002**, *89*, 186802.

[15] C. Putz, *Master thesis*, Johannes Kepler Universität, Austria, **2020**.

[16] N. D. Halim, A. W. Joseph, B. K. Lipska, *Journal of neuroscience methods* **2005**, *143*, 163.

[17] M. Li, I. Katsouras, C. Piliego, G. Glasser, I. Lieberwirth, P. W. M. Blom, D. M. de Leeuw, *J. Mater. Chem. C* **2013**, *1*, 7695.

[18] H. C. Woo, J. W. Choi, J. Shin, S.-H. Chin, M. H. Ann, C.-L. Lee, *The Journal of Physical Chemistry Letters* **2018**, *9*, 4066.

[19] J. Li, X. Yuan, P. Jing, J. Li, M. Wei, J. Hua, J. Zhao, L. Tian, *RSC Adv* **2016**, *6*, 78311.

[20] K. Wu, A. Bera, C. Ma, Y. Du, Y. Yang, L. Li, T. Wu, *Phys. Chem. Chem. Phys.* **2014**, *16*, 22476.

[21] S. M. Lee, C. J. Moon, H. Lim, Y. Lee, M. Y. Choi, J. Bang, *J. Phys. Chem. C* **2017**, *121*, 26054.

[22] C. R. Kagan, C. B. Murray, M. Nirmal, M. G. Bawendi, *Physical review letters* **1996**, *76*, 3043.

[23] M. A. Koc, S. N. Raja, L. A. Hanson, S. C. Nguyen, N. J. Borys, A. S. Powers, S. Wu, K. Takano, J. K. Swabeck, J. H. Olshansky et al., *ACS Nano* **2017**, *11*, 2075.

[24] M. V. Pavliuk, D. L. A. Fernandes, A. M. El-Zohry, M. Abdellah, G. Nedelcu, M. V. Kovalenko, J. Sá, *Advanced Optical Materials* **2016**, *4*, 2004.

[25] Y.-C. Hsiao, T. Wu, M. Li, B. Hu, *Adv. Mater.* **2015**, *27*, 2899.